

HST IMAGING OF THE HOST GALAXIES OF HIGH REDSHIFT RADIO-LOUD QUASARS¹

Matthew D. Lehnert^{2,3}

Sterrewacht Leiden, Postbus 9513, 2300 RA Leiden, The Netherlands

Wil J. M. van Breugel

Institute of Geophysics & Planetary Physics, Lawrence Livermore National Laboratory,
L-413 P.O. Box 808, Livermore, CA 94550

Timothy M. Heckman

Department of Physics and Astronomy, Johns Hopkins University, Baltimore, MD 21218

and

George K. Miley

Sterrewacht Leiden, Postbus 9513, 2300 RA Leiden, The Netherlands

Received; accepted

¹Based on observations with the NASA/ESA *Hubble Space Telescope*, obtained at the Space Telescope Science Institute, which is operated by the Association of Universities for Research in Astronomy, Inc., under NASA contract NAS5-26555.

²Participating Guest, Institute of Geophysics & Planetary Physics, Lawrence Livermore National Laboratory, L-413 P.O. Box 808, Livermore, CA 94550

³Current address: Max-Planck-Institut für extraterrestrische Physik (MPE), Postfach 1603, D-85740 Garching, Germany, mlehnert@mpe.mpg.de

ABSTRACT

We present rest-frame UV and Ly α images of spatially-resolved structures (‘hosts’) around five high-redshift radio-loud quasars obtained with the WFPC2 camera on the Hubble Space Telescope. The quasars were imaged with the PC1 through the F555W (‘V’-band) filter, which at the redshifts of the quasars ($2.1 < z < 2.6$) have central wavelengths of $\lambda_{rest} \approx 1500\text{\AA} - 1800\text{\AA}$, and at rest-frame Ly α using appropriately chosen narrow-band filters with the WFC2. The objects were selected from ground-based imaging surveys. Those had shown that many radio loud quasars at high redshift have prominent host galaxies which appeared to have properties similar to those of high redshift radio galaxies. Our HST observations allow a more detailed investigation of quasar host morphologies and a comparison with similar HST studies of radio galaxies by others.

Using several methods to measure and quantify the host properties we find that all five quasars are extended and this “fuzz” contains $\approx 5-40\%$ of the total continuum flux and $15-65\%$ of the Ly α flux within a radius of about $1.5''$. The rest-frame UV luminosities of the hosts are $\log \lambda P_\lambda \approx 11.9$ to $12.5 L_\odot$ (assuming no internal dust extinction), comparable to the luminous radio galaxies at similar redshifts and a factor 10 higher than both radio-quiet field galaxies at $z \sim 2 - 3$ and the most UV-luminous low redshift starburst galaxies. The Ly α luminosities of the hosts are $\log L_{Ly\alpha} \approx 44.3 - 44.9 \text{ erg s}^{-1}$ which are also similar to the those of luminous high redshift radio galaxies and considerably larger than the Ly α luminosities of high redshift field galaxies. To generate the Ly α luminosities of the hosts would require roughly a few percent of the total observed ionizing luminosity of the quasar.

The UV continuum morphologies of the hosts appear complex and knotty at the relatively high surface brightness levels of our exposures (about $24 \text{ V mags arcsec}^{-2}$). In two quasars we find evidence for foreground galaxies which confuse the host galaxy morphologies and which are responsible for some of the perceived radio/optical mis-alignments observed in ground-based imaging data. We do find good alignment between the extended Ly α and the radio sources, strong evidence for jet-cloud interactions in two cases, again resembling radio galaxies, and what is possibly the most luminous radio-UV synchrotron jet in one of the hosts at $z=2.110$. We discuss the significance of jet-cloud collisions in radio-loud quasars and their influence on radio morphologies in the frame work of simple orientation-based quasar/radio galaxy unification schemes.

Our observations suggest that the host galaxies of radio-loud steep spectrum quasars are similar to those of radio galaxies and strengthen previous conclusions

based on ground-based data that both types of objects are probably members of the same parent population.

Subject headings: Galaxies: evolution — galaxies: jets — quasars: host galaxies
— radio continuum: galaxies

1. Introduction

It is no exaggeration to say that between redshifts of $\approx 2-3$ to the present, highly luminous ($M < -26$) quasars have become virtually extinct. The co-moving space density of luminous quasars has fallen by about a factor of 1000 between these two epochs (*e.g.*, Hartwick & Schade 1990; Boyle 1993). What processes led to such a strong density evolution of highly luminous active galactic nuclei (AGN)? The answer to this question not only has important ramifications for our understanding of the AGN phenomenon, but will almost certainly give us important insight into the processes that controlled the evolution of galaxies in general since the “quasar epoch”.

It is an intriguing possibility that there is a strong link between the fueling of luminous AGN and galaxy formation. Indeed, the quasar epoch occurs at the time “Cold Dark Matter” models identify as when typical present-day galaxies were hierarchically assembled via dissipative mergers. Rees (1988), without regard to any specific cosmogony, argues that the process of galaxy formation was still continuing at the epoch $z=2$. This is especially true of the theoretical models where galaxy formation is a slow, diffuse, low-luminosity process (*e.g.*, Baron & White 1987; Kauffmann, White, & Guiderdoni 1993; Baugh et al. 1998). These general speculations therefore give a special prominence to high redshift AGN by hypothesizing that only when the proto-galactic material is energized by the luminosity of an AGN will it have high enough surface brightness to be readily detectable in emission-line surveys. In turn, the process of galaxy formation may be substantially altered by the effect of the AGN.

Observations of radio-loud quasars are also valuable for what we can learn about the AGN phenomenon in general. In particular, the relationship between radio-loud quasars and radio galaxies is of considerable interest, especially in light of efforts to “unify” these two classes through differences in viewing angle, environment, or evolutionary state (*e.g.*, Barthel 1989; Norman & Miley 1984; Neff & Hutchings 1990). In particular, the “viewing angle” scheme of Barthel (1989) in which radio-loud quasars and radio galaxies are drawn from the same parent population but viewed preferentially at small or large angles, respectively, to the radio axis, predicts that the luminosity and color of the quasar host should be very similar, if not identical, to those of the radio galaxies at similar radio powers and redshifts. Moreover, radio galaxies at high redshifts ($z > 0.6$) exhibit the so-called “alignment effect” (McCarthy et al. 1987; Chambers et al. 1987) where the radio, and the rest-frame UV and optical axes are all roughly co-linear. Recently, through the use of broad-band HST imaging data, it has become clear that quasars do indeed exhibit the “alignment effect” (Lehnert et al. 1999a) and that the effect in quasars is weaker than that seen in radio galaxies, as expected in simple orientation-based unification schemes (Lehnert et al. 1999b in preparation).

Radio-loud quasars at redshifts of 2-3 have impressively large and luminous continuum and emission-line nebulae (“hosts”; Heckman et al. 1991a,b; Lehnert et al. 1992). These structures comprise about 3% to over 40% of the total flux from the quasar and have Ly α luminosities of $\approx 10^{44-45}$ ergs s $^{-1}$, absolute visual magnitudes of about -25 , blue spectral energy distributions consistent with those of nearby late-type galaxies (Sc and Irr), and sizes of the order of many tens of kiloparsecs. Ground-based images of high- z radio loud quasars contain only limited morphological information (1 arc second seeing corresponds to about 11 kpc at these redshifts) and their morphology can best be described as asymmetric. Host galaxies of low-redshift quasars (*e.g.*, Boroson & Oke 1984; Boroson, Persson, & Oke 1985; Smith et al. 1986) have emission-line luminosities much lower than this (about 10^{42} ergs s $^{-1}$ in [OII]), spectral energy distributions similar to late-type galaxies, and absolute magnitudes of around -22 . However, Bahcall et al. (1994, 1995a,b) have recently concluded using HST WFPC2 images that the host galaxies of some of the brightest, low-redshift QSOs have wide range of host luminosities, with perhaps a large fraction of quasars hosts having luminosities $< L_*$. However, subsequent re-analysis of the data show that the host galaxies of low redshift quasars are in fact large luminous galaxies (McLeod & Rieke 1995; Bahcall et al. 1997). In spite of this, the properties of host galaxies of quasars have clearly evolved very strongly from high-redshifts (Kotilainen, Falomo, & Spencer 1998; Lehnert et al. 1992).

As tantalizing as the data and information contained in these studies of high redshift quasars are, there are some serious limitations to the usefulness of our previously obtained ground-based data. It is essential to be able to separate the strong nuclear emission of the quasar (continuum and Ly α) from that of its surrounding host. This can be most easily accomplished with the HST. Accurate separation of the quasar nucleus from its surrounding emission (within 10-20 kpc) allows us to address a number of issues which are of importance to our understanding of the evolution of luminous quasars, the association and similarity between high-redshift radio galaxies and radio-loud quasars, and the role of the large-scale radio emission in exciting and enhancing the extended line emission. To these ends, we used the HST to study a small subset of high-redshift, radio-loud quasars from our ground-based sample (Heckman et al. 1991a).

In this paper we represent an analysis of these observations, using several different methods to test the robustness of our results, and compare the quasar host properties with those of radio galaxies. Throughout this paper we adopt $H_0 = 50$ km s $^{-1}$ Mpc $^{-1}$, $q_0 = 0.1$, and $\Lambda = 0$ for easy comparison to previously published work on high redshift radio galaxies.

2. Observations and Reduction

The HST observations of our sample were made from September 1994 through May 1995 using the Wide Field Planetary Camera 2 (WFPC2). Each quasar was centered on the PC and was observed for a total of 2100 seconds (3×700 seconds) through the F555W filter (which closely corresponds to a ground-based V filter). In addition, we obtained exposures of 5000 seconds (5×1000 seconds) using the Wide Field Camera (WFC) and one of the Quad [OII] filters. The narrow-band filter was selected such that its central wavelength corresponded closely to the wavelength of redshifted Ly α from each of the quasars. The observations are summarized in Table 1. The pixel size is $0.046''$ pixel $^{-1}$ in the PC and $0.1''$ pixel $^{-1}$ in the WFC. The individual exposures were reduced using the standard pipeline reduction. The final images were produced by averaging the individual exposures with sigma-clipping to remove cosmic rays.

The bandpass of the telescope + WFPC2 + F555W combination covers the wavelength range of approximately 4500\AA and 6000\AA . The strong UV lines of CIV λ 1550, HeII λ 1640, and CIII] λ 1909 are included in this bandpass and in principle it is possible that these lines contribute to the detected extended emission. However, Heckman et al. (1991*b*) and Lehnert & Becker (1998) have shown that these lines are generally weak in quasar hosts, with the possible exception of PKS 0445+097. For this quasar Heckman et al. (1991*b*) found that the host has a HeII λ 1640 equivalent width of several \AA . From this and the brightness of the host in our PC image we estimate that HeII emission contributes much less than 1% to the total emission seen in the PC image. Thus the contribution of line emission to the total emission observed from the host in the F555W filter is negligible, for PKS 0445+097 and all other quasars in our sample.

The broad-band data were flux-calibrated assuming the inverse sensitivity for the F555W filter of 3.459×10^{-18} ergs s $^{-1}$ cm $^{-2}$ \AA^{-1} dn $^{-1}$ and a zero point of 22.563 (Whitmore 1995). This puts the resultant magnitudes on the ‘‘Vega system’’. To convert to the STMAG system, which assumes a flat spectral energy distribution and has a zero point of 22.543, 0.020 magnitudes should be subtracted from the magnitudes given here.

3. Image Reduction

3.1. Construction and Systematics of the PSF

We have attempted to quantify the shape and constancy of the HST PSF. First, we have collected images of the standard stars used to calibrate the F555W filter and observations

of bright stars in the outer regions of ω Cen that were made within a period of days of our observations. We found about 20 stars that were suitably close in time and within about 100 pixels of the central pixel of the PC (all of quasar images were centered near the middle of the PC CCD). We then constructed an empirical point-spread function using these data by adding the individual exposures after they had been aligned to a common center. This empirical PSF was then compared with the model PSF constructed using the PSF modeling program, “Tiny Tim”. However, the close agreement is limited to azimuthal averages – Tiny Tim does not reproduce the detailed 2-dimensional structure of the PSF (there is an asymmetry in the intensity of the diffraction spikes, especially in the +U3 direction, which Tiny Tim does not reproduce well). Next, we also measured the encircled energy diagrams (EEDs), i.e., the fraction of flux from a point source interior to a radius r , as a function of r . We then inter-compared all the EEDs taken through a given filter to determine the reproducibility of the EED and compared the individual stellar EEDs with that of the model PSF produced by Tiny Tim. We found very good agreement between the shape of the EED from the sum of the observations of standard stars and that of the Tiny Tim PSF. We then compared individual star EEDs with that of the Tiny Tim PSF. This inter-comparison of approximately 20 stars showed that we can detect host that contributes more than about 5% as much light as the quasar itself (within a radius of about $1.4''$). This limit is consistent with the known temporal variations in the HST PSF due to effects like the gentle change in focus over times scales of months and shorter time scale variations due to the so-called “breathing” of the telescope (see Burrows et al. 1995). We have restricted ourselves to radii less than about $1.5''$, to avoid the effect of the poorly understood large angle scattering which becomes important beyond a radius of about $2''$.

3.2. Host Measurements: PSF Subtraction

Measuring the properties of the circum-nuclear emission is important if we are to gain true insight into the properties of quasar host galaxies. One arc second at the redshift of quasars corresponds to roughly 11 kpc (in the cosmology: $H_0=50 \text{ km s}^{-1} \text{ Mpc}^{-1}$ and $q_0=0.1$ which will be used throughout this paper) – which is similar to the sizes of present-day galaxies. Thus being able to accurately subtract the nuclear emission of the quasar from the more extended emission is critical if we are to obtain information about the host of high redshift quasar on scales a fraction of the present-day galaxy size. We attempted this subtraction using two different PSFs. In the first, we modeled the PSF using the HST PSF modeling program, Tiny Tim. The second method was to construct a PSF by averaging several images (40s integrations) of a bright star in the outer regions of ω Centauri using the F555W and the PC. These stellar images were all within about 100 pixels of the center

of the PC chip and thus near the location of the quasar image on the PC chip. The images were aligned to the nearest pixel before averaging and the individual images covered the central 200 pixels of the planetary camera. The counts in the central pixel was about 2500 DN, comparable to that in the images of the quasars. We restricted ourselves to these observations and not the entire 20 that were used in the EED analysis. The subsample we used were chosen to sample the range of PC positions covered by the F555W quasar exposures as part of this program.

These two PSFs were iteratively subtracted until emission due to the diffraction of the secondary support was zero. This procedure allowed us to estimate the uncertainty in our fraction of extended emission by observing the points where the diffraction spikes became negative due to over subtraction of the PSF or were obvious in the PSF subtracted image due to under subtraction. We estimate that the range of possible acceptable amounts of PSF subtraction lead to a factor of 30% or ± 0.3 magnitudes in the quoted flux from the host. We note that these diffraction spikes were seen only out to about $1''$ in the PC frames and there was very little underlying nuclear emission from the quasar over most of this area. Using the model from Tiny Tim or the images of the star in ω Cen gave very similar results (*i.e.*, very similar fraction of the emission that was extended and similar morphology of the underlying emission). Therefore throughout the remainder of the paper, we will quote only the results of PSF subtraction obtained by subtracting the image of the star through the F555W and the PC.

The narrow-band images of the quasars generally only reveal modest extended emission. Using the efficiencies of the telescope, detector and filter combination made available by STScI and the integration time, we calculate that the scaling factor necessary to remove the continuum contribution to the narrow-band filter using the F555W filter to be about 50 – 100. Therefore continuum subtraction has only negligible effect on the properties of the extended emission. Unfortunately, we could not empirically measure this scaling factor. This is because the Quad [OII] filters only cover one of the WFCs at a time and in each of the images of the quasars, the stars available for such an estimate were either too faint to be useful, or were too bright and were saturated in the F555W image. To continuum subtract the narrow-band data, we block-averaged the PC continuum images 2×2 to make the scale of the PC continuum images match that of the WFC narrow-band images. The two images were then aligned and the F555W image then scaled by the factor calculated above. The final image is referred to as the Ly α image. The fluxes measured in the Ly α images are in reasonable agreement (always within a factor of 2) with those obtained from the ground by Heckman et al. (1991a).

The number of stars available for the construction of empirical PSF for the narrow-band

frames was very limited. However, each individual star used for the construction had many times the counts in the images of the quasars and therefore, even with just a few stars, the signal to noise in the final PSF was sufficient to make a reasonable subtraction of the PSF. We note that in none of the cases did a strong point source appear in the images and thus the method of PSF subtraction was a little bit different from the subtraction of the continuum images. None of the narrow-band images of the quasars had obviously visible diffraction spikes and thus most of the extended emission is little effected by the structure of the PSF. We therefore subtracted until the emission from the central peak roughly blended in with the more extended emission (*i.e.*, the subtraction did not cause a hole in the position of the nucleus). In Table 2, we quote the results of the PSF subtraction.

3.3. Host Measurements: Other Methods

We attempted several other techniques for estimating the amount of extended emission from each quasar. One relied on scaling the PSF such that its flux in the central 2 pixels matched that of the quasar image. We then took the ratio of the total energy encircled in apertures of increasing radius. This method provides an estimate of the minimum amount of extended flux in each quasar. The other technique we used to make this estimate was to cross-correlate a series of galaxy models plus PSF (to represent the underlying galaxy and quasar) with the image of the quasar. This technique was developed in a series of papers (Phillips & Davies 1991; Boyce, Phillips, & Davies 1993). Complete descriptions of the technique and its robustness can be found in the original papers cited above. We made this comparison with a series of model elliptical galaxies of varying half-light radii and ellipticities. Since we and the referee found that given the complexity of the host morphology revealed in the point-spread-function subtracted images, these other methods were perhaps not as convincing as the PSF subtraction. Thus, we will not go into detail of the results of these other methods. It is sufficient to say that they gave estimates very similar to those obtained through PSF subtraction.

4. Results

Contour plots of the HST images of all 5 quasars are shown in Figure 1. To compare the optical and radio structures we also overlaid high resolution radio maps from Lonsdale, Barthel, & Miley (1993) on the HST images, as shown in Figure 2. For these overlays, the coordinates from the HST images are insufficiently accurate to directly overlay the images using the coordinates given by the standard pipeline reduction. There is an uncertainty of

0.5'' to 1'' between the absolute HST positions as given by the pipeline reduction and the radio coordinate system. Therefore, we made some assumptions about how to position the radio images relative to the HST images. Using published spectral information available for these quasars, we identified the flattest spectrum component in each radio image, which is presumably associated with the radio AGN, and aligned that component with the most intense pixel (*i.e.*, the optical quasar nucleus) in the HST image. Second, we checked that our core determined using the method just outlined agreed with the astrometry from Barthel (1984) between high resolution VLA radio maps and the position of the quasar and in every case we found good agreement.

4.1. Notes Individual Objects

4.1.1. *PKS 0445+097*

The continuum image of PKS 0445+097 is rather asymmetric and one can discern two components: an asymmetric circum-nuclear host within $\sim 1''$ of the nucleus, elongated along P.A. $\approx 240^\circ$, and a detached “blob” at $\sim 2''$ from the nucleus at P.A. $\approx 120^\circ$. The host has a total magnitude of about 22.1 ± 0.3 magnitudes through the F555W filter. This “blob”, located about $1.5''$ (~ 17 kpc) to the east-southeast of the quasar nucleus, has a total magnitude of 23.1 ± 0.2 and is composed of several bright clumps immersed in a more diffuse structure. At surface brightness levels of ≈ 23 m_{F555W} arcsec^{-2} , its total extent is approximately 2.5×1.5 arc seconds (along PAs of $35^\circ \pm 10^\circ$ and $125^\circ \pm 20^\circ$). There is hint of a faint tail of emission leading from the region about the quasar nucleus out toward this blob of emission to the east-southeast. Another interesting feature in the circum-nuclear continuum emission is a $\sim 1''$ long “arc” of emission that curves out eastward of the nucleus and bends to the southeast. The total extent of the circum-nuclear emission, down to surface brightness levels of 23 m_{F555W} arcsec^{-2} , is about 2.5×0.8 arc seconds (roughly along PA = 105° and PA = 15° ; 30 kpc \times 9 kpc for $z=2.110$). The total extended emission (both the circum-nuclear host and blob to the southeast) comprises about 25% of the total emission seen from PKS 0445+097 in the F555W filter. The circum-nuclear host contributes about 17% of the total and the blob to the southeast of the nucleus about 7%.

The F555W continuum image is qualitatively and quantitatively consistent with the broad-band continuum images from Lehnert et al. (1992). These ground-based images show that the extended emission is blue (consistent with that of a nearby Irregular or Sc galaxy) and extended on spatial scales of about 8 arc seconds (~ 100 kpc) to the southeast (Lehnert et al. 1992). The HST image does not show as large of an extent, only about 2 – 3 arc seconds, but the orientation of the host is similar and the relative fraction of extended emission is

the similar (15 – 40% in the ground-based data). The HST image is more sensitive to the high surface brightness and more compact structures while the ground-based images with their inferior spatial resolution and larger projected pixel sizes, are more sensitive to the low surface brightness and more diffuse emission. This being the case, inspection of the HST F555W and our previously published ground-based images (Lehnert et al. 1992) suggests that both high surface brightness areas – the circum-nuclear host and the blob of emission – are embedded in a diffuse area of emission on scales of tens of kpc preferentially oriented along the axis southeast to northwest but also having some low surface brightness to the north, northeast, and southwest of the nucleus.

The narrow-band image of PKS 0445+097 is peculiar. The flux of the brightest source in the image is lower by a factor of ~ 100 than what we would have expected compared to the flux measured in a ground-based image (Heckman et al. 1991a). The filter we used for the narrow-band imaging of PKS 0445+097 is unusual in one respect compared to the other filters. In the filter holder, the FQUVN-A filter is located within the beam of the planetary camera. To move the filter onto one of the wide-field camera arrays, required the filter holder to be rotated 33° . We attribute the discrepancy in the measured flux to an unknown error in the positioning of the filter or of the target and for the remainder of the paper, we will not consider the narrow-band image of PKS 0445+097 further.

4.1.2. *MRC 0549-213*

The continuum image of MRC 0549-213 reveals a complex structure surrounding the quasar nucleus. The emission is symmetric about the nucleus, with the principal axis of the emission changing from about 90° within a few tenths of an arc second of the position of the nucleus, to a position angle of about 150° at a distance of $1''$. The total magnitude of the quasar (nucleus plus host) is about 19.7 and the magnitude of the host is about 21.3 ± 0.3 magnitudes in the F555W filter. The fraction of the total brightness contributed by the host is about 23%. In addition, we see a complex structure of continuum emission about 3.2 arc seconds to the west of the nucleus. This emission region has a curved arc shape and is approximately $1''$ in size, down to surface brightness levels of $\approx 23 \text{ m}_{F555W} \text{ arcsec}^{-2}$. It has a total magnitude of about 24.0.

The F555W continuum image is qualitatively and quantitatively consistent with the U band continuum image in Heckman et al. (1991). The ground-based U image shows that host is very extended, with the near-nuclear emission (within a few arc seconds of the nucleus) being preferentially oriented along $\text{PA} \approx 150^\circ$. Moreover, there is a “tail” of emission that extends about 5 arc seconds to the west. This morphology agrees quite well with that seen

in our F555W continuum image. Comparing the ground-based and HST image in detail suggests that the emission from the near-nuclear environment of the quasar and the blob to the west must actually be physically connected (deep R-band images of MRC 0549-213 obtained as part of another ground-based program shows a very similar morphology). Our HST image is not sufficiently deep to detect this connection. Also, the ground-based data suggested that about 20% of the U band flux is extended, consistent with the 23% estimated from our HST data.

The narrow-band image of MRC 0549-213 shows extended structure. Within a few tenths of an arc second of the nucleus, the emission is extended along $PA \approx 45^\circ$. On a scale of a few arc seconds there are two regions of significant emission. One is along $PA \approx 170^\circ$ and extends out about an arc second from the nucleus. About 1.6 arc second to the east of the quasar nucleus, there is a faint blob of emission that seems to be connected to the quasar nucleus proper. This faint blob of $Ly\alpha$ emission is approximately 1 arc second long in the north-south direction and about 0.5 arc seconds wide in the east-west direction down to our detection limit. The flux from this distinct region of emission is 9.7×10^{-16} ergs s^{-1} cm^{-2} . In addition, we see several areas of low surface brightness emission near this object. Two regions are particularly noteworthy. One area corresponds to the blob 3.2 arc seconds to the west. There is a $\approx 4 \sigma$ region of $Ly\alpha$ emission over the region of this blob. Also, there is some $Ly\alpha$ emission roughly corresponding to a area of continuum emission about 3 arc seconds away from the nucleus along $PA \approx 325^\circ$. Unfortunately, there does not exist a ground-based $Ly\alpha$ image of this quasar with which to compare.

4.1.3. *PKS 1318+113*

The continuum image of PKS 1318+113 shows two concentrations of emission, one immediately surrounding the quasar nucleus and the other about 2 arc seconds to the east of the quasar nucleus. Immediately surrounding the quasar nucleus (within about $1''$), the emission is asymmetric, with the brighter isophotes oriented along $PA \approx 135^\circ$ and the fainter isophotes are most extended along $PA \approx 180^\circ$ to 200° . The total magnitude of the quasar is about 19.0 in the F555W filter and the host has a magnitude of about 20.1. This implies that the host makes up about 38% of the total emission from the quasar (nucleus + host). We note that perhaps this is somewhat over-estimated in light of the fact that the cross-correlation technique implies that only about 19% of the quasar light is extended. The galaxy to the east of the nucleus has a magnitude of about 21.9 (measured in a $2'' \times 2''$ box, which is as large as can be used due to the proximity of this galaxy to the line-of-sight of the quasar). Down to surface brightness levels of ≈ 24 m_{F555W} $arcsec^{-2}$, the extent of the circum nuclear

host is about 1 to 1.5 arc seconds.

The HST F555W image is similar to the B-band image presented from Heckman et al. (1991a). The ground-based image shows bright extended emission to the east of the nucleus, with fainter emission to the south and west. The total extent of the ground-based B image is about 6 - 10'' from the nucleus. The HST image does not reveal emission quite as extended as this, only about 2 – 3 arc seconds, but the gross characteristics of the host is similar. The relative fraction of extended emission between the ground-based and HST data are not very similar (16% in the ground-based B data versus about 38% in the HST F555W data; although we note that the cross-correlation analysis gives 19%; see Table 2). This suggests that relatively speaking, the light from the host is concentrated within an 1'' of the nucleus (scales not available from the ground). Although again, we note that the cross-correlation analysis gives a result much more consistent with our previous ground-based results.

The narrow-band image of PKS 1318+113 shows extended emission (Figure 1). Most of the extended Ly α emission is to the north and east of the nucleus, primarily along PA \approx 45° and is extended on 1'' to 2'' from the nucleus (down to surface brightnesses of 6.3×10^{-16} ergs s $^{-1}$ cm $^{-2}$ arcsec $^{-2}$). There are several faint regions of emissions within a few arc seconds of the quasar. These regions have fluxes of roughly 1.7 to 7.1×10^{-16} ergs s $^{-1}$ cm $^{-2}$. Moreover, we find reasonable agreement with the morphology of the ground-based Ly α image presented in Heckman et al. (1991a). In the ground based Ly α images the host was extended along PA \approx 45° with the most extended emission being on the southwest side of the nucleus. Detailed comparison between the ground-based and HST Ly α images suggest that the highest surface brightness emission is on the northeast side of the nucleus with several bright clumps of the southwest side that is then embedded in a halo of diffuse Ly α emission.

One of the most remarkable results of this small HST survey of the host galaxies of high redshift quasars is the interesting spatial relationship between extended Ly α and radio jet emission. In Figure 2, we show an overlay of the Ly α HST image and a VLA A-array map from Lonsdale et al. (1993). We see that the jet passes between two Ly α emitting blobs southwest of the quasar nucleus. This interaction appears at the point where the jet appears to bend. The two blobs have total fluxes of 1.67×10^{-16} ergs s $^{-1}$ cm $^{-2}$ and 2.01×10^{-16} ergs s cm $^{-2}$ for the eastern-most and western-most emission regions. Measuring the sizes of these blobs, we find that the eastern most blob is approximately circular with a diameter of 0.3''. The western most blob of the two is approximately 1'' \times 0.35'' (long versus short axis oriented PA \approx 150°). We also note that there seems to be another region of Ly α emission along the “counter-jet” side of the quasar between the nucleus and the north-eastern radio lobe.

4.1.4. 1658+575 (4C 57.29)

The continuum image of 1658+575 (4C 57.29) shows a relatively compact (about 1'' across) region of extended emission. The total magnitude of the quasar (nucleus + host) is 18.3 and the magnitude of the host is 20.0. We find that about 21% of the total emission from the quasar is extended. We see a linear feature along $PA \approx 150^\circ$ in the extended emission. This feature is very likely to be a residual emission that was not accounted for during PSF subtraction. This is not surprising since 1658+575 is the brightest quasar imaged during this program and hence had the most extended and intense diffraction spikes compared to the other quasar images. Ignoring the linear feature we see that the brightest emission is north and to the southwest of the nucleus. The diameter of the host is only about 1'' down to surface brightnesses of $22 \text{ m}_{F555W} \text{ arcsec}^{-2}$.

The ground-based B band image of 1658+575 presented in Heckman et al. (1991a) shows a structure roughly similar to that observed using the HST. The quasar is extended on scales of about 10'' in the ground-based image and has a high surface brightness region to the east-southeast of the nucleus with lower surface brightness emission also to the north-northeast and south of the nucleus.

The narrow-band image of 1658+575 shows an extended plume of emission to the north-east with some very significant emission also extended to the northwest of the nucleus. There is also a lower surface brightness extension to the south of the nucleus. The most extended emission reaches a radius of about 2'' from the nucleus. Comparison with the ground-based Ly α image of Heckman et al. (1991a) again reveals a very strong similarity between the two images. In the ground-based data Ly α is extended on scales of up to 6'' from the nucleus. The most significant of this extended emission is to the northwest through the south side of the nucleus.

4.1.5. PKS 2338+042

The host galaxy of the quasar PKS 2338+042 comprises nearly 40% of the total continuum emission from the quasar. The host is asymmetric with an “arm” of emission that emanates from the nucleus to the south and then bends around to the east. In addition, there is a “plume” of emission to the northeast of the nucleus. The total extent of the continuum nebula is about 1.5'' down to a surface brightness of $24.0 \text{ m}_{F555W} \text{ arcsec}^{-2}$. The circular contour seen 0.4'' to the east of the nucleus in the contour plot is a local minimum in the emission.

The 15 GHz radio map of Lonsdale et al. (1993) shows a “bent” core, jet, double

lobe source oriented preferentially in an east-west direction. The “jet” emanates from the nucleus along $PA \approx 90^\circ$, with the hotspot of the eastern lobe is at $PA \approx 120^\circ$. The western hotspot is at $PA \approx 270^\circ$. Overlaying this map onto the PSF subtracted HST image, we see a close correspondence between features in the HST image and that of the radio image. The maximum intensity seen in the contour plot of the radio emission just to the east of the nucleus along the “jet” corresponds to the local minimum we see in the contour plot of the F555W image. This local minimum gives the impression that we are looking down the end of a hollow tube of emission which contains the radio emission. Farther to the east we see that the surface brightness of the continuum emission increases at roughly the same point where the jet seems to “bend” towards the hotspot. Moreover, we notice that the rest-frame UV isophotes of the F555W image seem to bend outwards to the west of the nucleus approximately along the same position angle as that to the western radio lobe (*i.e.*, $PA \approx 270^\circ$).

The F555W continuum image is roughly consistent with the ground-based 4m image taken through the B-filter by Heckman et al. (1991). This ground-based image shows the most significant emission is to the southeast of the nucleus and is extended about $6''$ across down to a surface brightness of $27.3 m_B \text{ arcsec}^{-2}$. The HST image does not reveal emission quite as extended as this, only a few arc seconds, but the orientation of the host is roughly similar. The HST image however suggests that a much greater fraction of the emission is extended, namely $\sim 40\%$ versus $\sim 16\%$ from the ground-based B image. The HST image is obviously more sensitive to the high surface brightness and more compact structures while the ground-based images with their inferior spatial resolution and larger projected pixel sizes, are more sensitive to the low surface brightness and more diffuse emission. This would suggest that perhaps Heckman et al. (1991) over-subtracted the ground-based image of PKS 2338+042 and that the UV continuum host of PKS 2338+042 is very compact compared to the rest of this small sample.

The $\text{Ly}\alpha$ image of PKS 2338+042 is also very extended, revealing a host galaxy approximately $2''$ across down to a surface brightness of $5.4 \times 10^{-16} \text{ ergs s}^{-1} \text{ cm}^{-2} \text{ arcsec}^{-2}$. The morphology of the host galaxy in $\text{Ly}\alpha$ is similar to that of the continuum emission. The basic orientation of the $\text{Ly}\alpha$ host is east-west. The most significant piece of the morphology of this image is an “arm-like” structure that extends from the nucleus out to about 1 arc second to the east where it terminates in a relatively high surface brightness region of emission. To the north of this “arm” there is a region of relatively low surface brightness compared to its immediate surroundings (a “hole” in the extended emission). There are fainter “plumes” of emission to the northeast and the south-southeast. At the lowest surface brightness visible in the $\text{Ly}\alpha$ image, there is also a faint extension to the northwest. At the lowest surface brightness levels, the orientation of the $\text{Ly}\alpha$ is preferentially in the southeast-northwest direction

($PA \approx 140^\circ$) as opposed to the general east-west orientation at higher surface brightnesses.

The morphology of the HST Ly α image is similar to that seen in the ground-based Ly α image of Heckman et al. (1991). The ground-based Ly α image shows a general southeast-northwest orientation with Ly α emission being seen over about $9''$. The ground-based Ly α image is of course a much deeper image than our HST Ly α image, reaching down to a surface brightness of 1.5×10^{-17} ergs s $^{-1}$ cm $^{-2}$ arcsec $^{-2}$.

Overlaying the 15 GHz radio image of Lonsdale et al. (1993) on the HST Ly α image we again see a good correspondence between the highest surface brightness Ly α emission and the radio “jet”. The Ly α shows a high surface brightness extension about $0.8''$ to the east of the nucleus. Over this same region the jet of radio emission is observed. It is interesting that over the region of the most intense extended Ly α emission is also the region where we see the “jet” of radio emission and where the radio emission undergoes its most severe bending (in projection). Moreover, we again see that to the west of the nucleus, the isophotes “bend” outwards from the nucleus over a region about $0.5''$ out from the nucleus. This is along the same position angle from the nucleus that we see the most distant radio hotspot

To elucidate the relationship between the radio and UV continuum and Ly α line emission, we have made a single cut through the 15 GHz radio image from Lonsdale et al. (1993), and both the PSF subtracted F555W and narrow-band Ly α image (which has not been PSF subtracted). These cuts were made from the highest surface brightness peak in the nucleus of the radio image, in the PSF subtracted F555W, and in the Ly α image and then including all the pixels to the east and west of the nucleus out to a radius of roughly an arc second in both directions. We have normalized and overlaid these cuts in Figure 3. The direction of the cut was selected such that it passed directly along the radio jet that points directly to the east of the nucleus so that we may directly compare the one-dimensional spatially extended radio, UV continuum, and Ly α radial distributions.

As can be seen in this Figure, the radio and UV continuum emission are strongly correlated, while the radio and Ly α emission are not. Since this projected cut lies along the direction of the minimum in the spatial distribution of the UV continuum (see Figure 1), the top panel of Figure 3 shows that the jet must pass through the local minimum (best described as a “hole”) in the distribution of the UV continuum emission. On the other hand, the anti-coincidence of the radio and Ly α distribution is such that at the position where the jet is bending away to the southeast, which is why the radio surface brightness in the bottom panel of Figure 3 is decreasing, the Ly α surface brightness is increasing and reaching a local maximum. The spatial relationship between the Ly α and radio emission is very suggestive of a “jet-cloud” interaction in that the area of high surface bright Ly α emission is responsible for bending the jet.

While the structure of the Ly α image is rather complex, to aid us in interpreting the data in relationship to a possible “jet-cloud” interaction, we wish to estimate the flux from the region of relatively high surface brightness in the Ly α image at the point where the jet bends to the southeast. Isolating the pixels over this region (approximately $0.3'' \times 0.3''$ region about $0.8''$ from the nucleus), we find a total Ly α flux of 2.1×10^{-16} ergs s $^{-1}$.

5. Discussion

In this section we discuss the results and their implications for our understanding of the circum-nuclear environments of high redshift quasars. Our sample is too small for a detailed statistical analysis. Thus, we will focus our attention on a few commonalities shared by the quasar hosts and compare these properties with those of high redshift radio galaxies and field galaxies, and low redshift starburst galaxies.

5.1. The Radio-Aligned UV Continuum and Confusion by Intervening Absorber Galaxies

Heckman et al. (1991a) and Lehnert et al. (1992), from ground-based images of quasars, found weak evidence for alignment between the rest-frame optical/UV and the radio emission. In a HST/WFPC2 snapshot study of 43 quasars from the 3CR catalog, Lehnert et al. (1999b) argue that quasars hosts indeed exhibit the “alignment effect” in the continuum plus line emission (all of the broad-band HST images in that study have some contribution due to emission lines) but that the effect is slightly weaker than in radio galaxies at similar redshifts. As discussed below, the HST data show that intervening galaxies along the line of sight to the quasar may confuse the morphologies of the hosts: 2 of the 5 quasars from our sample appear to have nearby galaxies seen in projection (PKS 0445+097 and PKS 1318+113). Interestingly, these two quasars were precisely those which showed the greatest mis-alignment between the rest-frame UV continuum host and radio emission in the study of Heckman et al. (1991a).

The evidence that PKS 0445+097 has a nearby intervening system SE of the nucleus is based on Keck 10m spectroscopy (Lehnert & Becker 1998), as well as morphological and luminosity considerations. The Keck spectrum shows that the SE blob is at a redshift of 0.8384 ± 0.0002 , which is similar to that of the MgII absorption seen against the nuclear continuum of PKS 0445+097 (Barthel, Tytler, & Thompson 1990). Therefore, it is not surprising that we found no Ly α emission from this “blob” at the redshift of the quasar.

In addition, Lehnert & Becker also found that this galaxy is likely to contain a Seyfert 2 nucleus. If we adopt $z=0.84$ for the redshift of this galaxy, the central wavelength of the F555W filter corresponds to about 2930\AA in the rest-frame of the galaxy. This wavelength is close to the wavelengths of the U and B filters and thus extrapolations from flux density measured in the F555W to estimate the flux densities of the U and B filters in the rest-frame of the quasar host are small. Using the spectral energy distribution from Armus et al. (1997) for this galaxy (approximately that of a late-type spiral) to extrapolate the measured flux density in the F555W filter to the flux density at the wavelengths of the U and B filters in the rest-frame of the intervening galaxy and correcting for Galactic extinction, we find that the U and B absolute magnitude of the blob to the SE of the nucleus is $M_U = -21.8$ and $M_B = -21.3$. Thus this intervening galaxy is approximately a factor of 2 more luminous than a fiducial Schechter L^* galaxy.

Moreover, this intervening galaxy appears to have a very distorted morphology. The HST F555W image shows a galaxy with three knots of emission elongated along $PA \approx 45^\circ$ with the brightest region not roughly in the center of the emission but towards the northeastern end of the galaxy. The galaxy appears to be nearly edge-on. Comparing the morphology of this galaxy with other intervening absorbers observed with the HST (*e.g.*, Dickinson & Steidel 1996; Steidel et al. 1997), we find that the galaxy along the line of sight to PKS 0445+097 is peculiar. Most MgII absorbing galaxy have properties consistent with the general field population of galaxies and hence “normal” morphologies and distributions of luminosity similar to field galaxies (Steidel et al. 1997; Bergeron & Boisse 1991; Steidel et al. 1994). However, many of the peculiar morphologies appear to be associated with galaxies that are viewed nearly edge-on (Dickinson & Steidel 1996). Thus we conclude that even though the morphology appears to be peculiar compared to most MgII absorbing galaxies, its apparently edge-on orientation implies that extinction in the disk may account for its seemingly peculiar morphology. The two color analysis of Armus et al. (1997) suggests that the color of this galaxy is consistent with Sc spiral galaxy at $z=0.84$ with about 0.5 magnitudes of additional extinction compared to low redshift Sc spiral galaxies. This additional reddening is consistent with our claim here that extinction may account for this galaxy’s seemingly peculiar morphology. However, it could also be that since this galaxy appears to be harboring a Seyfert nucleus (Lehnert & Becker 1998), it might also be that the complex morphology is associated with a merger event that initiated the Seyfert activity.

In the case of PKS 1318+113 no direct spectroscopic evidence exists that its companion to the east is also a foreground object. If this object is at the redshift of the quasar, it would have an implausibly high luminosity ($> 25 L^*$ and more luminous than the quasar host). There are several other more plausible possibilities for the redshift of this object. The two most plausible redshifts for this object, 0.8388 and 1.0541, which are associated with Mg

II absorbers along the line of sight to PKS 1318+113 (Barthel et al. 1990; Jankarkarinen, Hewitt, & Burbidge 1991). Since this galaxy is bright (about 21.9 in F555W), it is more likely that this galaxy is associated with the MgII absorber at $z=0.8388$, which is very similar to the case of PKS 0445+097. The absolute magnitude of this galaxy under the same assumptions made previously for the absorber along the line of sight to 0445+097 implies $M_U \approx -23$ and $M_B \approx -22.5$. These magnitudes are many L^* and thus we consider associating this galaxy with the MgII absorber at $z=0.8388$ very implausible and that it is associated with the absorber at $z=1.0541$ even less likely (see e.g., Bergeron & Boisse 1991; Steidel et al. 1994). However, such a speculation will have to await spectroscopic observations to determine the redshift of this nearby (in projection) galaxy.

5.2. The Nature of the UV Continuum

We will center our discussion of the UV continuum in the hosts of quasars on two aspects: the origin of radio-aligned UV continuum and the stellar population of the underlying galaxy.

5.2.1. The Radio-Aligned Component

There have been a few hypotheses for the physical causes of extended UV continuum emission in high redshift quasars and radio galaxies. The most viable ones are: 1) star formation stimulated by the radio jet as it propagates outwards from the nucleus (McCarthy et al. 1987; Chambers et al. 1987; De Young 1989; Rees 1989; Begelman & Cioffi 1989), 2) scattering of light from a hidden quasar by electrons or dust (e.g., Fabian 1989; Cimatti et al. 1997), 3) inverse Compton scattering of microwave background photons by relativistic electrons in the radio jets or lobes (Daly 1992a; b), and 4) selection effects related to the possible enhancement of radio emission by dense gas which is preferentially located along the galaxy’s major axis (Eales 1992). Observing that in fact the radio and UV continuum on small scales are anti-correlated (see also Lehnert 1996), meaning that the high surface brightness radio emission from the jet is actually in a minimum in the rest-frame UV, provides a test of these various proposed schemes.

In the model of jet induced star-formation and scattering hypothesis, we might expect to see such anti-correlations on small scales in addition to the “alignment” between the radio and UV continuum emission. This might come about for the same reason in both cases. The pressure from the jet would push material outwards both along the jet and perpendicular to it. The high perpendicular pressure might cause clouds to become unstable and collapse

and it would also clear material from the region of the jet. In case of the jet-induced star-formation hypothesis, overpressure due to the passing jet might cause these clouds to form stars and in the scattering hypothesis, the over-pressurized clouds would provide for more efficient scattering of the quasar light. In both hypotheses, this would explain the large scale relationship (*i.e.*, the “alignment effect”) but on small scales (*i.e.*, the width of the jet) a anti-coincidence whether generated by star-formation or scattering. However, since it is difficult to understand how the jet can inhibit stars from moving into the regions through which it passes, the jet-induced star-formation scenario only works if the crossing time of the high mass stars is much longer than their evolutionary time scale. Otherwise, the massive stars that are formed at the edge of the jet will fill in the jet region with high surface brightness UV emission. If the time scale for the massive stars to penetrate into the region of the jet is long enough, the massive stars will die out, thus preserving the “hole” in the light through which the jet is passing. Interestingly, the radio source in PKS 2338+042 is likely to be young; its observed small radio size (roughly a 10-20 kpc, modulo projection effects) suggests that it is only between 10^6 and 10^7 years old which is roughly the same order of magnitude as the evolutionary time scale of high mass stars. For example, if the stars are orbiting at 100 km s^{-1} , they will transverse 1 kpc (0.1” at the redshift of the quasar in the adopted cosmology) in about 10^7 years. The scattering hypothesis does not suffer from such a draw back and is feasible with the only caveat that the jet must be fairly efficient at removing possible scatterers from the regions through which it is passing. Given that the pressure in the jet is estimated to be many orders of magnitude higher than the reasonable pressure of the ISM in a normal galaxy (like the Milky Way for example), such a possibility seems highly plausible.

The suggestion of Inverse Compton scattering seems to be ruled out by these observations. Inverse Compton scattering of microwave background photons by relativistic electrons in the radio jets or lobes (Daly 1992a; b), would in fact require that the regions of the highest electron density (likely to be the jets) should have the highest UV surface brightnesses. This is exactly the opposite of what we observed.

Assigning the “alignment effect” to possible selection effects related to the enhancement of radio emission by dense gas which is preferentially located along the galaxy’s major axis (Eales 1992) is an interesting suggestion that seems plausible given the current data set. We have found evidence for “jet cloud” interactions in 2 out of the 4 sources imaged at $\text{Ly}\alpha$ (see §5.3.1). Therefore strong interactions between the radio and ambient interstellar medium are certainly not rare in radio galaxies or quasar hosts (§5.3 and references therein). Within this context, it may be that the “hole” in the UV continuum may be related to the increased pressure in the region surrounding the jet due to the passage of the jet that in fact prevents it from de-collimating. However, in order to gauge whether or not this speculation is plausible

will require more extensive observations.

To make this discussion more generic, we note that other quasar hosts appear to have this general alignment, but exhibit detailed spatial anti-coincidence between the radio and rest-frame UV emission (although perhaps not as dramatic as that seen in PKS 2338+042). In HST snapshot data on a large sample of quasars selected from the 3CR sample, Lehnert (1996) found evidence for subtle anti-correlation between radio and rest-frame UV continuum and line emission in these sources (also see de Vries et al. 1996) even though generally the radio emission “aligned” with the rest-frame UV continuum and line emission. These anti-coincidences were mainly seen in the sources with complex compact morphologies, roughly similar to the radio morphology of PKS 1318+113 and PKS 2338+042.

5.2.2. A Possible Radio-UV Synchrotron Jet in PKS 0445+097

As has been emphasized previously, an important issue in the study of high redshift radio-loud AGN is the relationship between the relativistic radio-emitting plasma and the line and continuum emission from the host galaxies. To test this hypothesis, we have overlaid a 0.16'' resolution image of PKS 0445+097 from Lonsdale et al. (1993) on the F555W image (Figure 2). Here we have assumed that the bright, compact eastern component is identified with the quasar nucleus on the basis of its inverted radio spectrum ($\alpha_{5GHz}^{15GHz} = -0.6 \pm 0.2$; Barthel 1984). The overlay shows that there is a curved optical feature southwest of the quasar which corresponds to the radio jet. The optical and radio flux densities in a 0.5×0.5 arc second area centered on this feature are $0.18 \pm 0.04 \mu\text{Jy}$ ($\lambda_{obs} = 5398 \text{ \AA}$, the center of the F555W filter) and $13.5 \pm 0.7 \text{ mJy}$ ($\lambda_{obs} = 2.0 \text{ cm}$), implying a spectral index ($S_\nu \sim \nu^{-\alpha}$) of $\alpha_R^O = 1.1 \pm 0.2$. This is consistent with a steepening radio-optical synchrotron spectrum since the radio spectral index of the jet between 5 GHz and 15 GHz is $\alpha_{5GHz}^{15GHz} = 0.8 \pm 0.2$ (Barthel 1984) and suggests that the emission may indeed be associated. If this is true, and deep HST imaging polarimetry would be required to prove this, then the optical jet in PKS 0445+097 would be the most luminous and highest redshift jet known (in the rest-frame of the quasar: $\log L_B = 29.0 \text{ ergs s}^{-1} \text{ Hz}^{-1}$ and $\log P_{1.4GHz} = 34.6 \text{ ergs s}^{-1} \text{ Hz}^{-1}$, more than an order-of-magnitude more luminous than any previously discovered synchrotron jet; see Dey and van Breugel 1994 for a discussion of known optical/radio synchrotron jets). However, considering the complex and filamentary structure of the circum-nuclear host, there is of course also the possibility that the optical/radio association is accidental, and the α_R^O fortuitously close to the value expected for synchrotron emission. We note also that the 5 GHz map of PKS 0445+097 published by Barthel (1984) shows a small extension northeast from the core, *i.e.*, opposite to the southwest radio jet, and coincident with the optical extension in that same

direction seen in the HST image. No radio spectral index information for this feature is available.

5.2.3. *Star Forming Regions in the Quasars Hosts?*

If the circum-nuclear UV continuum from the hosts are due to recent star formation, than it is of interest to compare the UV luminosities with low redshift starburst and normal galaxies (Kinney et al. 1993; Donas et al. 1987; Treyer et al. 1998). We find that the typical luminosity of the circum-nuclear host is about $10^{12} L_{\odot}$ at $\approx 1700\text{\AA}$ (λP_{λ} ; Table 3), compared to $\lesssim \text{few} \times 10^{11} L_{\odot}$ for normal and starburst galaxies at low redshift ($H_0=50 \text{ km s}^{-1} \text{ Mpc}^{-1}$). Thus the host galaxies of quasars are at least an order of magnitude more luminous than the most luminous low redshift galaxies in the UV. However, Calzetti, Kinney, & Storchi-Bergmann (1994) and Meurer et al. (1997) find the typical UV extinction in the Kinney et al. sample and starbursts generally to be about 1-3 magnitudes at $\approx 1700\text{\AA}$. If we correct the most extreme UV-emitting galaxies in the local universe for this amount of UV extinction, they can indeed reach the UV luminosities observed in the circum-nuclear hosts of the quasars. Therefore analogs for the circum-nuclear host associated with these quasars may exist in the local universe, but must be the most extreme UV-luminous galaxies and, moreover, the quasar hosts must be relatively unobscured. There is no good reason to assume why the latter should be the case.

To add some further perspective on the nature of the hosts of radio loud quasars, we note that the UV luminosity of the hosts measured in this study are much more luminous than the “Lyman drop-out” field galaxies studied by by Steidel and collaborators (Steidel et al. 1996; Giavalisco, Steidel, & Macchetto 1996). Using the UV (1500\AA) luminosity function for Lyman drop-out galaxies presented by Dickinson (1998), we find that the average UV luminosity of these 5 quasar hosts is about a factor of 10 more luminous than the most luminous Lyman drop-out galaxies. This comparison was made without correcting either sample for the effects of dust extinction. Therefore, it is difficult to associate quasar hosts with the field population of starburst galaxies at high redshift – even the extremely luminous ones.

5.3. **The Extended Ly α Emission**

Our quasars typically have Ly α luminosities of $\approx \text{few} \times 10^{44} \text{ ergs s}^{-1}$. Ly α luminosities this high are typical of what is observed in high redshift radio galaxies (*e.g.*, van Oijk et

al. 1997; McCarthy 1993). This suggests that quasars and high redshift radio galaxies have similar galaxy-scale environments and ionizing sources, and supports models which attempt to unify radio galaxies and quasars through orientation, evolution, and environment. In addition, even in our relatively short HST exposures, the Ly α emission is extended over tens of kpc; again very similar to what has been observed in high redshift radio galaxies. These results are in agreement with the conclusions of our other investigations of high redshift ($z > 2$) quasar hosts (*e.g.*, Heckman et al. 1991a, b; Lehnert & Becker 1998).

However, quasars offer us an advantage over the radio galaxies. Since we can observe the nucleus more directly, we can estimate the observed ionizing flux emitted by the quasar nucleus. Using the measured UV fluxes from the HST data and using the scaling relations between the flux of UV wavelengths and the total ionizing energy in quasars from Elvis et al. (1994), we estimate that in order to produce the Ly α emission observed, the host galaxy intercepts only a few percent of the total ionizing luminosity of the quasar. This is not surprising considering the observations of the “proximity effect” in the Ly α forest lines. The “proximity effect”, where the number density of Ly α forest lines is lower near the quasar than away from it (*e.g.*, Weymann, Carswell, & Smith 1981; Bechtold 1994), has been interpreted as the hydrogen becoming more highly ionized within the sphere of influence of the quasar. Observing this effect implies that much of the ionizing radiation from quasars must escape to cluster scales and thus the host galaxy of the quasar cannot be completely optically thick to ionizing photons in all directions. This is in agreement with our estimate that the host galaxy and immediate environment of the quasar nucleus only intercepts a few percent of the total ionizing luminosity. Of course it could be less since there could be local sources of ionization such as young stars and/or shocks generated by the mechanical power from the radio jets. To determine the relative importance of local ionization sources would require spatially resolved spectroscopy.

The radio/Ly α overlays (Fig. 2) show that there is a good association between the radio emission and the structure of the Ly α emission. First, the principal axis of the radio emission is generally along the same direction as the extended Ly α emission. This is very similar to the radio-aligned extended emission-line regions seen in high redshift radio galaxies (*e.g.*, McCarthy 1993 and references therein). Second, the surface brightness of the line and radio emission appear anti-correlated to some degree (see *e.g.*, Fig. 2). This is generally seen at the point where the jet and radio emission are curved. Third, it seems that the brightest Ly α and radio emission are on the same side where the radio lobe is closest to the quasars. This resembles the radio/emission-line asymmetry correlation found for radio galaxies by McCarthy, van Breugel, & Kapahi (1991). All of these properties may be best understood as being due to strong interaction of the radio sources (jets and lobes) with dense, asymmetrically distributed ambient gas. Numerous examples of this are known in nearby

radio galaxies (*e.g.*, 3C277.3: van Breugel et al. 1985; 3C 405 and 3C 265: Tadhunter 1991; 3C 356: Eales & Rawlings 1990; PKS 2152-699: Fosbury et al. 1998; PKS 1932-464: Villar-Martin et al. 1998; 3C 171: Clark et al. 1998).

5.3.1. “Jet-Cloud Collisions”

Our observations show two good examples in which jet-cloud collisions seem to occur: PKS 1318+113 and PKS 2338+042. In the case of PKS 1318+113 we observe two emission-line regions between which the radio jet is passing. At this same location the radio jet bends. This radio/optical morphology is very similar to that seen in some nearby radio galaxies, especially Minkowski’s Object (van Breugel et al. 1985) and is strongly suggestive of a jet cloud interaction. In PKS 2338+042 the spatial resolution is insufficient to allow a similarly detailed examination but the co-spatial bright Ly α and radio knots east of the quasar and the radio jet curvature downstream from this location suggest a similar jet-cloud collision occurs in this object.

By analogy to the radio galaxies we will briefly examine whether the observed cloud properties are consistent with such an interpretation. With the limited data in hand (*i.e.*, without high spatial resolution spectroscopy) we can explore only few of the consequences expected from a violent jet-cloud collision. The main questions we can address are 1) are the clouds massive enough to deflect the jets, and 2) can they survive the collisions on time-scales comparable to the radio source ages?

The two Ly α blobs SW of the quasar nucleus in PKS 1318+113 have $L_{Ly\alpha}=1.1\times 10^{43}$ ergs s $^{-1}$ and $L_{Ly\alpha}=1.3\times 10^{43}$ ergs s $^{-1}$ to the east and west of the radio emission respectively. Assuming no dust, pure case B recombination for 10,000 K (Osterbrock 1989), cylindrical or spherical symmetry, and using the projected isophotal dimensions apparent in the Ly α image as discussed previously, we then find that $n_e^2 f_V \sim 0.5$ for both blobs, where n_e is the electron density and f_V is the volume filling factor. Since we do not have data to estimate either n_e or f_V independently, we must rely on estimates obtained for other objects. Rough estimates of the volume filling factors for the extended emission line regions in various radio galaxies suggest $f_V \sim 10^{-4}$ to 10^{-6} and $n_e \sim 10 - 1000$ cm $^{-3}$ (see *e.g.*, Baum et al. 1992; McCarthy 1993; Lacy & Rawlings 1994). If for convenience we assume $n_e = 100$ cm $^{-3}$, then this would imply a volume filling factor of about 5×10^{-5} and thus consistent with values found by previous studies. These estimates would then imply a mass of ionized material in these clouds of about $\text{few} \times 10^7 (n_e/100 \text{ cm}^{-3}) (f_V/10^{-4}) M_\odot$. Making similar assumptions for the Ly α emission-line regions in PKS 2338+042, we find that $n_e^2 f_V \sim 1$ and would thus estimate that the mass of the clouds must be $\approx 10^8 (n_e/100 \text{ cm}^{-3}) (f_V/10^{-4}) M_\odot$. We note

that the above estimates would be similar if we assumed that the gas were shock heated instead of implicitly assuming that the gas is in recombination equilibrium since most of the Hydrogen line emission comes predominately from the post-shock recombination zone (*e.g.*, Dopita & Sutherland 1992).

Are such masses capable of deflecting the radio jets emanating from the nuclei? Theoretical modeling suggests that jets can be deflected by discrete objects, but only if certain minimal criteria are met. First and foremost, the deflector must be sufficiently massive as so not to be pushed out of the way of the radio jet too quickly. Following the arguments in Icke (1991) and McNamara et al. (1996), we estimate that deflecting clouds must have a mass, $M_{cloud} \gtrsim 6 \times 10^4 M_{\odot} \left(\frac{0.1}{\eta}\right) \left(\frac{L_{rad}}{10^{42} \text{ ergs s}^{-1}}\right) \left(\frac{c}{v_{jet}}\right) \left(\frac{1 \text{ kpc}}{l_{jet}}\right) \left(\frac{t_{jet}}{10^6 \text{ yrs}}\right)^2$, such that it has not moved away by more than the length of the undeflected jet, l_{jet} , during the lifetime of the radio source, t_{jet} , and where η is the conversion efficiency of the jet power, P_{jet} , into radio emission such that $L_{rad} = \eta P_{jet}$, and v_{jet} is the velocity of the jet. From the characteristics of the radio emission given in Barthel (1984), we estimate that the radio luminosity of PKS 1318+113 is about $4 \times 10^{43} \text{ ergs s}^{-1}$ and of PKS 2338+042, $7 \times 10^{43} \text{ ergs s}^{-1}$ and the ages of both sources is likely to be of-order 10^6 to 10^7 yrs (*e.g.*, Alexander & Leahy 1987). Using these estimates we see that the mass necessary to resist being pushed out of the way is about $10^8 M_{\odot}$ (assuming $\eta = 0.1$, $v_{jet} = 0.2c$, $l_{jet} = 1 \text{ kpc}$, and $t_{jet} = 10^6 \text{ yrs}$). Our rough mass estimates above suggest that the clouds in PKS 1318+113 and PKS 2338+042 are sufficiently high for these clouds to be able to resist the pressure of the radio jets for the relatively short time that they have likely endured the passage of the radio jet.

Can the cloud survive the impact from a powerful jet? In both sources we observe what appear to be discrete clouds at the point where the radio jets are deflected. This suggests that a significant portion of the clouds must have survived the impact in order to remain visible; although perhaps the cloud in PKS 1318+113 has been split or had a hole drilled through it. The clouds, in absence of a confining external pressure, will likely be disrupted on a time-scale of the order a few times the sound crossing time. Taking the cloud to have a gas temperature of about 10^4 K , we estimate the sound speed $v_s = 15 \text{ km s}^{-1}$. For cloud sizes of 3-4 kpc (which is the approximate projected sizes of the clouds in our adopted cosmology), we then find that the sound crossing time of these clouds is of-order 10^8 yrs . This is much longer than the likely age of the jet, which is probably comparable or smaller than the radio source age which, for powerful double sources is estimated to be of order 10^6 to 10^7 yrs (*e.g.*, Alexander & Leahy 1987). Therefore we find, within the frame work of our assumptions, that there is no particular problem with seeing relatively intact, massive emission-line clouds millions of years after the jet-cloud collisions occurred.

The above calculations suggest that 1) quasar hosts may contain rather large amounts

of dense clouds and 2) that these can be very efficient at deflecting radio jets during a significant fraction of the total age of the source (*i.e.*, roughly 10^7 yrs). To make this argument more general, we note that we only observed good evidence for jet-cloud interaction in two sources, PKS 1318+113 and PKS 2338+042. In two other sources, PKS 1658+575 and MRC 0549-213 we did not see evidence for a jet cloud interaction, and in PKS 0445+097 we suspect that there is something wrong with the narrow-band observation (§4.1.1.). Thus, we see strong cloud-jet interaction in two of the four sources. However, PKS 1658+57 and MRC 0549-213 (and also PKS 0445+097) exhibit linear projected radio morphologies suggesting that no dense clouds intercept the jets in these objects; although there is a region of Ly α emission beyond the edge of the eastern radio lobe of MRC 0549-213 perhaps suggesting a large amount of confining material along that direction. Obviously a much larger sample of quasars with high resolution Ly α images are necessary before a statistically significant conclusion can be made. However, our observations strongly suggest that the bent radio structures in radio quasars may very well be due to the interaction of their jets with dense ambient gas (Barthel & Miley 1988) and that such interactions may be very common and may affect a large percentage of the total radio-loud high redshift quasar population.

5.3.2. *Relevance to Unification Schemes*

The Ly α and continuum images of PKS 2338+042 and the Ly α image of PKS 1318+113 show relatively obvious signs of interaction between the radio emitting plasma and ambient emission line gas and perhaps even with the stellar population (as probed by the UV continuum emission). These results suggest that the interaction between the radio and the ambient interstellar medium of the host galaxy and cluster-scale environment must be important. In fact, if we take our data literally, they imply that interaction with the ambient medium is important in determining the radio morphology in $\approx 1/2$ of the quasars. Clearly, a much larger sample of high redshift quasars need to be observed to determine the exact statistics of the impact of the structure of the host galaxy and cluster-scale environment in influencing the radio emission.

However, even for a limited number of quasars, this observation is important. Given that much of the evidence for orientation based unification relies on various aspects of the radio morphology of the sources (linear sizes, lobe arm length asymmetries, predominance of jets, etc) this result allows us to speculate that one would not expect there to be much evidence for orientation-based unification based on radio observations alone. **IF** interactions between the radio and inhomogeneities in the ISM of radio loud objects are important in determining (and limiting) the size and lobe asymmetries in radio sources, then such interaction might

dominate over the simple growth of the radio emission with time and orientation effects. Studies that use observations of linear sizes, lobe arm length asymmetries and bends and twists in the radio jets and lobes to test unification schemes (e.g., Gopal-Krishna, Kulkarni, & Whitta 1996; Kapahi et al. 1995) may in fact get statistically insignificant results not because orientation-based unification is incorrect, but because interactions between the relativistic radio plasma and the ambient ISM and IGM either dominates or provides a significant source of “noise” in the observations. This may partially explain why the results of tests of unification schemes using radio data have been so mixed and that orientation-based unification seems most appropriate for a rather limited range of redshifts and generally only for samples of relatively low redshift radio sources (see Barthel 1989 for example).

6. Summary and Conclusions

In this paper, we presented HST WFPC-2 images of spatially-resolved structures (‘hosts’) around five high-redshift radio-loud quasars. The quasars were imaged using the planetary camera with the broad-band F555W (‘V’) filter and in the wide field camera with a narrow-band filter whose central wavelength is approximately that of redshifted Ly α in each of the quasars. These radio-loud quasars were selected from the earlier imaging survey of quasar “host” by Heckman et al. (1991a) and Lehnert et al. (1992). These HST images confirm and extend our earlier ground-based results.

From an analysis of the images and a comparison with high resolution VLA radio images we conclude that:

- 1) All of the high redshift quasars are extended in both the rest-frame UV continuum and in Ly α . We find extended fractions that range from about 5% to 40% of the total continuum within a radius of about 1.5". In spite of the fact that these images have higher spatial resolutions and relatively short integration times on a small telescope, the morphological agreement between the ground-based images and these HST images is quite good. Moreover, there is reasonable agreement with our estimates of the fraction of the quasar light contributed by the host galaxies in both the HST and ground-based data. Such a result is surprising given the fact that the HST images reveal a wealth of structure within an arc second of the nucleus which is currently unattainable from the ground.
- 2) The typical integrated magnitude of the host is $V \sim 22 \pm 0.5$. The typical UV luminosity is roughly $10^{12} L_{\odot}$ (λP_{λ} , uncorrected for internal extinction), which is about a factor of 10 higher luminosity than that observed for the “Lyman drop out” field galaxies studied by Steidel and collaborators and the most UV luminous zero redshift starburst galaxies. The

$\text{Ly}\alpha$ images are also spatially-resolved. The typical luminosity of the extended $\text{Ly}\alpha$ is about $\text{few} \times 10^{44}$ ergs s^{-1} . These luminosities require roughly a few percent of the total ionizing radiation of the quasar.

3) Quasar host generally show “alignment” between the radio, $\text{Ly}\alpha$, and UV continuum emission. There is clear evidence that the gas “knows” about the radio source. This manifests itself in the “alignment” between the radio, $\text{Ly}\alpha$, and UV continuum emission, in detailed morphological correspondence in some of the sources which suggests “jet-cloud” interactions, and in the fact that the brightest radio emission and the side of the radio emission with the shortest projected distance from the nucleus occurs on the same side of the quasar nucleus as the brightest, most significant $\text{Ly}\alpha$ emission. These observations of jet-cloud interaction influencing the radio morphologies is a challenge to simple orientation based quasar/radio galaxy unification schemes. This is perhaps why the use of the radio morphology has generally lead to conflicting results when used to judge the appropriateness of orientation based quasar/radio galaxy unification schemes.

4) The high spatial resolution of the HST has revealed that objects along the line of sight but near the quasars in projection have made a significant contribution to the continuum light from these objects. We note in particular that 0445+097 and 1318+113 were two quasars with strong mis-alignment between the principal emission axes in the radio and the ground-based images at UV rest wavelengths (Heckman et al. 1991a). It is now clear that this mis-alignment was partially due to the contaminating effects of nearby (in projection; less than 2 arc seconds for the quasar nucleus) foreground galaxies.

The authors wish to thank Ray Lucas for his considerable help in making sure that our program went smoothly. Conversations about the complexities of the HST/WFPC2 PSF with Chris Burrows and John Krist were particularly helpful in making the most of the data. We thank the referee, Dr. Eric Smith, whose comments lead to a substantial improvement in the style and presentation of this paper and Dr. Greg Bothun for his conscientious handling of the manuscript in his role as the scientific editor. The work of MDL and WvB at IGPP/LLNL was performed under the auspices of the US Department of Energy under contract W-7405-ENG-48 and the work of MDL at the Sterrewacht Leiden was supported by funds provided by the Dutch Organization for Research (NWO). This work was supported in part by grant number GO-5393 from the Space Telescope Science Institute, which is operated by the Association of Universities for Research in Astronomy, Inc., under NASA contract NAS5-26555. We also acknowledge support from a NATO research grant.

REFERENCES

- Alexander, P. & Leahy, J. P. 1987, MNRAS, 225, 1
- Armus, L., Neugebauer, G., Lehnert, M. D., & Matthews, K. 1997, MNRAS, 289, 621
- Bahcall, J. N., Kirhakos, S., & Schneider, D. P. 1994, ApJ, 435, L11
- Bahcall, J. N., Kirhakos, S., & Schneider, D. P. 1995, ApJ, 447, L1
- Bahcall, J. N., Kirhakos, S., & Schneider, D. P. 1995, ApJ, 450, 486
- Bachall, J. N., Kirhakos, S., Saxe, D. H., & Schneider, D. P. 1997, ApJ, 479, 642
- Baron, E., & White, S. D. M. 1987, ApJ, 322, 585
- Barthel, P. 1984, Ph.D. thesis, Leiden University
- Barthel, P., Miley, G., Schilizzi, R., & Lonsdale, C. 1988, A&AS, 73, 515
- Barthel, P., & Miley, G. 1988, Nature, 333, 319
- Barthel, P. 1989, ApJ, 336, 606
- Barthel, P., Tytler, D., & Thompson, B. 1990, A&AS, 82, 339
- Baugh, C. M., Cole, S., Frenk, C. S., & Lacy, C. G. 1998, ApJ, 498, 504
- Baum, S. A., Heckman, T. M., & van Breugel, W. 1992, ApJ, 389, 208
- Bechtold, J. 1994, ApJS, 91, 1
- Begelman, M., & Cioffi, D. 1989, ApJ, 345, L21
- Bergeron, J., & Boisse, P. 1991, A&A, 243, 344
- Boroson, T. A., & Oke, J. B. 1984, ApJ, 281, 535
- Boroson, T. A., Persson, S. E., & Oke, J. B. 1985, ApJ, 293, 120
- Boyce, P. J., Phillips, S., & Davies, J. J. 1993, AA, 280, 694
- Boyle, B. J. 1993, in *The Environment and Evolution of Galaxies*, eds. H. A. Thronson and J. M. Shull, (Dordrecht: Kluwer), p. 433
- Calzetti, D., Kinney, A. L., & Storchi-Bergmann, T. 1994, ApJ, 429, 582

- Chambers, K., Miley, G., & van Breugel, W. 1987, *Nature*, 329, 604
- Cimatti, A., Dey, A., van Breugel, W., Hurt, T., & Antonucci, R. 1997, *ApJ*, 476, 677
- Clark, N. E., Axon, D. J., Tadhunter, C. N., Robinson, A., & O'Brien, P. 1998, *ApJ*, 494, 546
- Daly, R. A. 1992a, *ApJ*, 386, L9
- Daly, R. A. 1992b, *ApJ*, 399, 426
- de Koff, S., Baum, S. A., Sparks, W. B., Golombek, D., Biretta, J., Macchetto, D., McCarthy, P., & Miley, G. K. 1996, *ApJS*, 107, 621
- De Young, D. S. 1989, *ApJ*, 342, L59
- Dey, A. & van Breugel, W. J. M. 1994, *AJ*, 107, 1977
- de Vries, W. H., O'Dea, C. P., Baum, S. A., Sparks, W. B., Biretta, J., de Koff, S., Golombek, D., Lehnert, M. D., Macchetto, F., McCarthy, P., & Miley, G. K. 1997, *ApJS*, 110, 191
- Dickinson, M., & Steidel, C. C. 1996, in *New Light on Galaxy Evolution*, eds. R. Bender and R. L. Davies, (Dordrecht: Kluwer), p. 265
- Dickinson, M. 1998, preprint.
- Donas et al. 1987, *A&A*, 180, 12
- Eales, S. A., 1992, *ApJ*, 397, 49
- Eales, S. A., & Rawlings, S. 1990, *MNRAS*, 243, 1
- Elvis, M., Wilkes, B. J., McDowell, J. C., Green, R. F., Bechtold, J., Willner, S. P., Oey, M. S., Polomski, E., & Cutri, R. 1994, *ApJS*, 95, 1
- Fabian, A. 1989, *MNRAS*, 238, 41P
- Fosbury, R. A. E., Morganti, R., Wilson, W., Ekers, R. D., di Serego Alighieri, S., & Tadhunter, C. N. 1998, *MNRAS*, 296, 701
- Giavalisco, M., Steidel, C., & Macchetto, F. 1996, *ApJ*, 470, 189
- Gopal-Krishna, Kulkarni, V. K., & Witta, P. J. 1996, 463, 20

- Hartwick, F., & Schade, D. 1990, *ARA&A*, 28, 437
- Heckman, T. M., Lehnert, M. D., van Breugel, W. J. M., & Miley, G. M. 1991a, *ApJ*, 390, 100
- Heckman, T. M., Lehnert, M. D., Miley, G. K., & van Breugel, W. J. M. 1991b, *ApJ*, 381, 373
- Icke, V. 1991, in *Beams and Jets in Astrophysics*, ed P. A. Hughes, (Cambridge: Cambridge University Press), p. 232
- Junkkarinen, V., Hewitt, A., & Burbidge, G. 1991, *ApJS*, 77, 203
- Kapahi, V. K. , Athreya, R. M., Subrahmanya, C. R., Hunstead, R. W., Baker, J. C., McCarthy, P. J., & van Breugel, W. 1995, *A&AS*, 16, 125
- Kauffmann, G. White, S. D. M., & Guiderdoni, B. 1993, *MNRAS*, 264, 201
- Kinney, A. L., Bohlin, R. C., Calzetti, D., Panagia, N., & Wyse, R. F. G. 1993, *ApJS*, 86, 5
- Kotilainen, J. K., Falomo, R., & Scarpa, R. 1998, *A&A*, 332, 503
- Lacy, M. & Rawlings, S. 1994, *MNRAS*, 270, 431
- Lehnert, M. D., Heckman, T. M., Chambers, K. C., & Miley, G. K. 1992, *ApJ*, 393, 68
- Lehnert, M. D. 1996, in “The Second Workshop on Gigahertz Peaked Spectrum and Compact Steep Spectrum Radio Sources”, eds. I. Snellen, R. Schilizzi, H. Rottgering, and M. Bremer (Leiden: Leiden Observatory),
- Lehnert, M. D., & Becker, R. H. 1998, *A&A*, 332, 514
- Lehnert, M. D., Miley, G. K., Sparks, W. B., Baum, S. A., Biretta, J., Golombek, D., de Koff, S., Machetto, F. D., & McCarthy, P. J. 1999a, *ApJS* submitted
- Lehnert, M. D., de Koff, S., McCarthy, P. J., Miley, G. K., Baum, S. A., & Sparks, W. B., 1999b, in preparation
- Lonsdale, C., J., Barthel, P. D., & Miley, G. K. 1993, *ApJS*, 87, 63
- Lowenthal, J. D. 1991, Ph.D. thesis, University of Arizona
- McCarthy, P., van Breugel, W., Spinrad, H., & Djorgovski, S., 1987, *ApJ*, 321, L29
- McCarthy, P. J., van Breugel, W., & Kapahi, V. K. 1991, *ApJ*, 371, 478

- McCarthy, P. 1993, ARA&A, 31, 639M
- McCarthy, P., Miley, G. K., de Koff, S., Baum, S. A., Sparks, W. B., Golombek, D., Biretta, J., & Macchetto, D. 1997, ApJ, 112, 415
- McLeod, K. K., & Rieke, G. H. 1995, ApJ, 454, 77
- McNamara, B. R., Wise, M., Sarazin, G. L., Jannuzi, B. T., & Elston, R. 1996, ApJ, 466, L9
- Meurer, G. Heckman, T. M., Lehnert, M. D., Leitherer, C., & Lowenthal, J. 1997, AJ, 115, 54
- Neff, S., & Hutchings, J. 1990, AJ, 100, 1441
- Norman, C., & Miley, G. K. 1984, A&A, 141, 85
- Osterbrock, D. E. 1989, *Astrophysics of Gaseous Nebulae and Active Galactic Nuclei*, (Mill Valley, CA: University Science Books)
- Phillips, S., & Davies, J. J. 1991, MNRAS, 251, 105
- Rees, M. 1988, MNRAS, 231, 91P
- Rees, M. 1989, MNRAS, 239, 1p
- Smith, E., Heckman, T., Bothun, G., Romanishin, W., & Balick, B. 1986, ApJ, 306, 64
- Steidel, C. C., Dickinson, M., Meyer, D. M., Adelberger, K. L., & Sembach, K. R. 1997, ApJ, 480, 568
- Steidel, C. C., Giavalisco, M., Dickinson, M., & Adelberger, K. L. 1996, AJ, 112, 352
- Steidel, C. C., Pettini, M., Dickinson, M., & Persson, S. E. 1994, AJ, 108, 2046
- Tadhunter, C. N. 1991, MNRAS, 251, 46p
- Treyer, M. A., Ellis, R. S., Milliard, B., Donas, J., & Bridges, T. J. 1998, MNRAS, 300, 303
- Weymann, R. J., Carswell, R. F., & Smith, M. G. 1981, ARA&A, 19, 41
- Whitmore, B. 1995, in *Calibrating Hubble Space Telescope: Post Servicing Mission*, ed. A. Koratkar and C. Leitherer (Baltimore: Space Telescope Science Institute), p. 269
- Wide Field and Planetary Camera 2 Instrument Handbook, C. J. Burrows (Ed.), STScI Publication (June 1995)

van Breugel, W., Miley, G., Heckman, T., Butcher, H., & Bridle, A. 1985, ApJ, 290, 496

van Breugel, W., Filippenko, A. V., Heckman, T., & Miley, G. 1985, ApJ, 293, 83

van Ojik, R., Röttgering, H. J. A., Miley, G. K., & Hunstead, R. W. 1997, AA, 317, 358

Villar-Martin, M., Tadhunter, C., Morganti, R., Clark, N., Killeen, N., & Axon, D. 1998, A&A, 332, 479

FIGURE CAPTIONS

Fig. 1.— For each row of this plot, we show the F555W image with the PSF removed as described in the text on the right and the Ly α image is on the left, except for PKS 0445+097 for which we only display the image taken through the F555W filter. Each image has been rotated so that north is at the top and east is to the left and each has been smoothed using a 4×4 median filter. The faintest contours are listed in Table 2 and each contour is a factor of two increase in surface brightness. Each image is approximately $8'' \times 8''$ in projected size and the solid bar indicates the angular size of 10 kpc at the redshift of the quasar assuming $H_0=50 \text{ km s}^{-1} \text{ Mpc}^{-1}$, $q_0=0.1$, and $\Lambda = 0$.

Fig. 2.— We show the PSF subtracted F555W continuum or the narrow-band (grey-scale) with contours of the high-resolution VLA 2 cm radio map from Lonsdale et al. (1993) overlaid. In each of the plots the radio nucleus as determined in §4 has been centered to the position of the optical nucleus of the quasar. The Figures are specifically, a) F555W image of PKS 0445+097, b) F555W image of MRC 0549-213, c) narrow-band Ly α image of MRC 0549-213, d) F555W image of PKS 1318+113, e) narrow-band Ly α image of PKS 1318+113, f) F555W image of 1658+575 (4C 57.29), g) narrow-band Ly α image of 1658+575 (4C 57.29), h) F555W image of PKS 2338+042, and i) narrow-band Ly α image of PKS 2338+042.

Fig. 3.— At the top, we show the comparison of a one-dimensional light profile of the PSF subtracted F555W (rest-frame UV continuum) image of PKS 2338+042 compared to the one-dimensional radio intensity profile of the radio map from Lonsdale et al. (1993). Below, we show a similarly constructed comparison of the narrow-band Ly α light profile compared to the radio map of Lonsdale et al. (1993). Both 1-dimensional profiles are along right ascension which was chosen because it lies directly along the radio jet. The radio and HST images were aligned and scaled for this comparison. The flux scale is arbitrary and chosen for convenience in making the comparison of the light distributions at each wavelength.

Table 1. Observation Log

Quasar (1)	Filter (2)	FOV (3)	N (4)	Int (5)	Date (6)
0445+097	F555W	PC	3	700	11/09/94
	FQUVN33	WP2	5	1000	11/09/94
0549–213	F555W	PC	3	700	22/04/95
	FQUVN-D	WF2	5	1000	22/04/95
1318+113	F555W	PC	3	700	23/05/95
	FQUVN-B	WF4	5	1000	23/05/95
1658+575	F555W	PC	3	700	12/01/95
	FQUVN-B	WF4	5	1000	12/01/95
2338+042	F555W	PC	3	700	06/12/94
	FQUVN-C	WF3	5	1000	12/01/95

Note. — Col. (1) — Source designation. Col. (2) — Filter used for the observation. Col. (3) — The aperture used for the observation. “PC” is the planetary camera, and “WF2”, “WF3”, “WF4” are the wide field cameras 2, 3, and 4. Col. (4) — Number of separate exposures each with the exposure time in listed in Col. (5). Col. (5) — Integration time in seconds per exposure. Col. (6) — Date of observations in the form of day/month/year.

Table 2. Photometry of the Sources

Quasar (1)	m_{total} (2)	f(PSF-) (3)	Rotation (4)	SB limit (5)
0445+097	20.2	0.19	-62.6	24.1
	-15.1	...	26.9	...
0549-213	19.7	0.23	159.3	24.0
	-13.8	0.20	-111.2	-15.0
1318+113	19.0	0.38	173.7	24.0
	-13.8	0.18	84.1	-15.2
1658+575	18.3	0.21	9.5	23.0
	-13.5	0.16	-80.2	-15.2
2338+042	21.2	0.37	132.3	24.0
	-14.2	0.65	-47.8	-15.0

Note. — Col. (1) — Source designation. Col. (2) — Total magnitude in the F555W filter or the logarithm of the total Ly α flux (in units of ergs s⁻¹ cm⁻²) of the quasar. The total magnitude of the quasar in the F555W filter is listed in the first row for each object, while the logarithm of the total Ly α flux is enumerated in the second row. Col. (3) — Fraction of the total quasar light that is extended as indicated by PSF subtraction. Col. (4) — Angle (in degrees) that the image was rotated to make north at the top and east to the left in each image. Positive values imply a counter-clockwise direction of the rotation. To calculate the PA of the brightest diffraction spike one uses the following formula. If the rotation is positive, its rotation - 45°, if the rotation is negative, it is rotation - 45° + 360°. Col. (5) — Surface brightness limit of the lowest contour of the plots shown in Figure 1 in units of magnitudes arcsec⁻² for the continuum images and in units of the logarithm of ergs s⁻¹ cm⁻² arcsec⁻² for the Ly α images.

Table 3. UV Power and Ly α Luminosities

Quasar	z	λ_{rest}	$f_{\lambda,total}$	$f_{\lambda,fuzz}$	$\log \lambda P_{\lambda,tot}$	$\log \lambda P_{\lambda,fuzz}$	$\log L_{Ly\alpha,total}$	$\log L_{Ly\alpha,fuzz}$
(1)	(2)	(3)	(4)	(5)	(6)	(7)	(8)	(9)
0445+097	2.110	1740	−16.5	−17.2	12.6	11.9
0549−213	2.245	1660	−16.3	−17.0	12.7	12.0	45.3	44.5
1318+113	2.171	1700	−16.0	−16.5	12.9	12.4	45.0	44.3
1658+575	2.173	1700	−15.8	−16.4	13.1	12.5	45.3	44.5
2338+042	2.549	1520	−16.5	−17.0	12.8	12.3	45.1	44.9

Note. — Col. (1) — Source designation. Col. (2) — Redshift of the source. Col. (3) — The central wavelength of the F555W filter in the rest-frame of the quasar using 5397Å as the central wavelength of the F555W filter. Col. (4) — Flux density of the total emission from the quasars in units of the logarithm of $\text{ergs s}^{-1} \text{cm}^{-2} \text{Å}^{-1}$ at the wavelength given in col. (3). Col. (5) — Flux density of the “fuzz” in units of the logarithm of $\text{ergs s}^{-1} \text{cm}^{-2} \text{Å}^{-1}$ at the wavelength given in col. (3). Col. (6) — The logarithm of the UV power of the quasar taken to be λP_{λ} in units of solar luminosities using the rest wavelength given in col (3) and the assumed cosmology of $H_0=50 \text{ km s}^{-1} \text{ Mpc}^{-1}$ and $q_0=0.1$. We have also corrected for galactic extinction using the extinction in the B-band given in NED and using the standard extinction curve from Osterbrock (1989). The value of solar luminosity used to make the conversion is $L_{sun} = 3.83 \times 10^{33} \text{ ergs s}^{-1}$. Col. (7) — The UV power of the “fuzz” (λP_{λ}) in units of the logarithm of solar luminosities at the wavelength given in col. (3). The relative fraction of extended emission used in this calculation is from the PSF subtraction analysis (see Table 2 and text for details). Col. (8) — The total Ly α luminosity of the quasar in units of the logarithm of ergs s^{-1} . Col. (9) — The total Ly α luminosity of the “fuzz” in units of the logarithm of ergs s^{-1} . The relative fraction of extended emission used in this calculation is from the PSF subtraction analysis (see Table 2, cols. (2) and (3) for the fluxes used and text for details).

This figure "fig1a.gif" is available in "gif" format from:

<http://arxiv.org/ps/astro-ph/9904114v1>

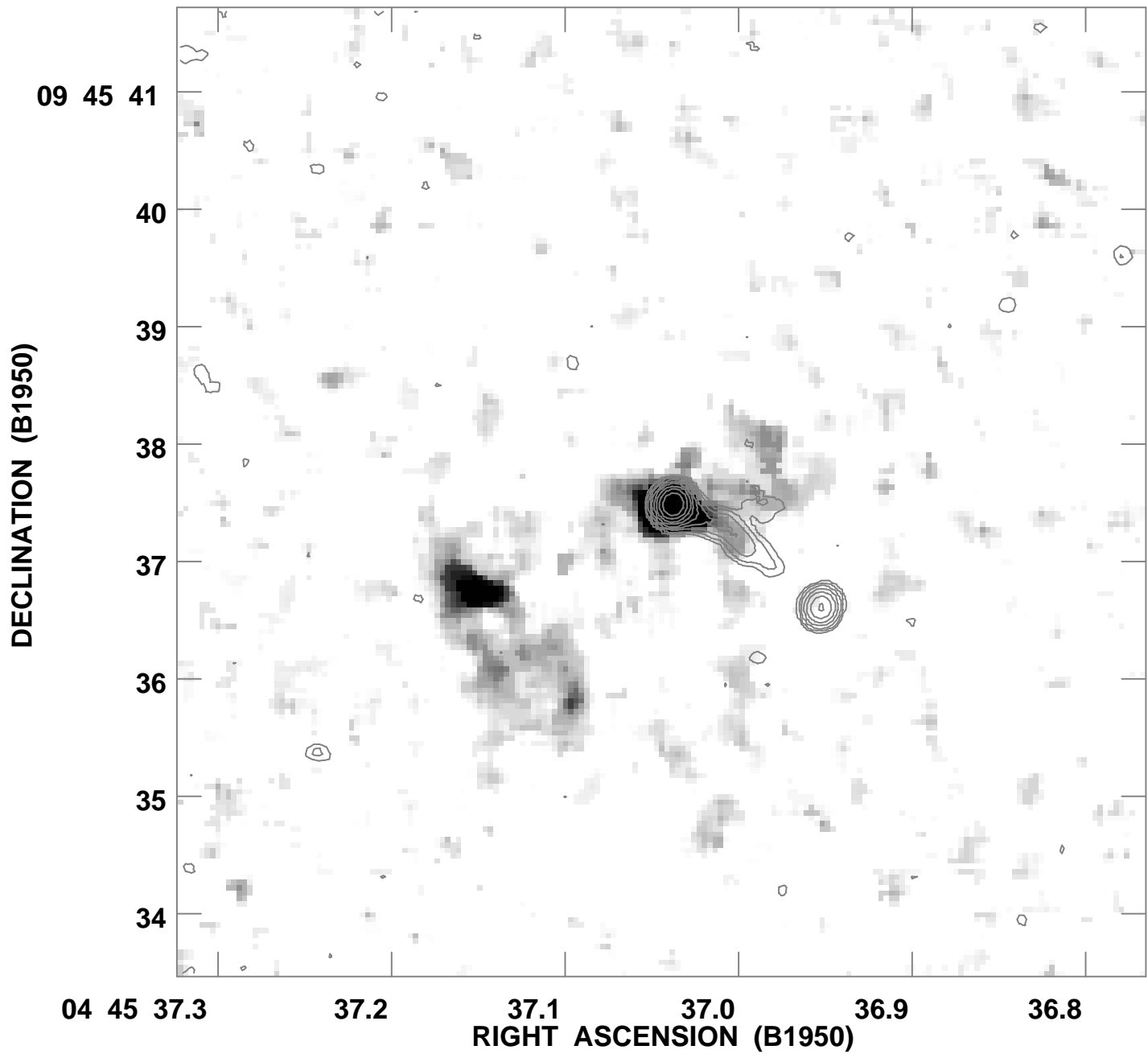
This figure "fig1b.gif" is available in "gif" format from:

<http://arxiv.org/ps/astro-ph/9904114v1>

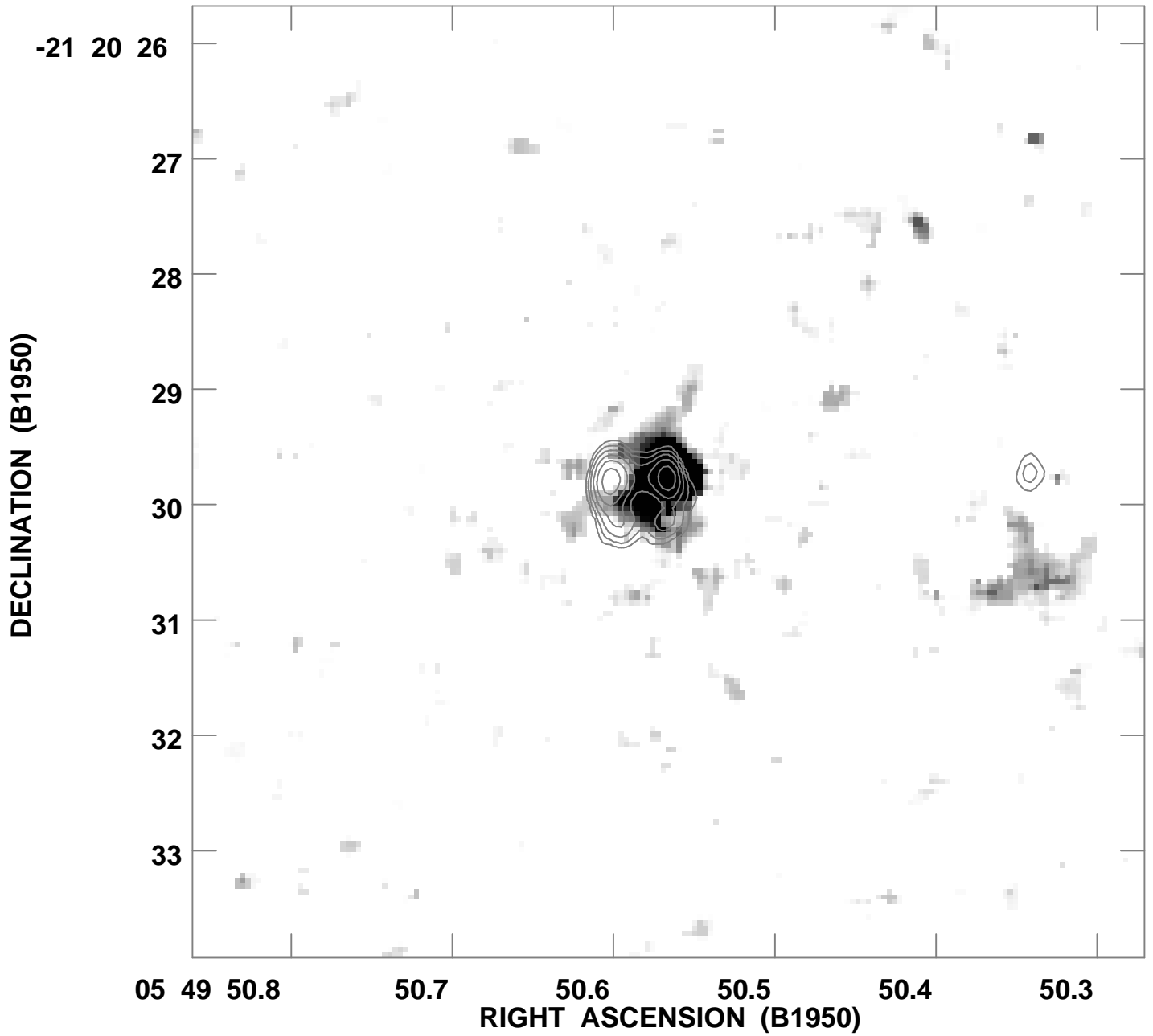
This figure "fig1c.gif" is available in "gif" format from:

<http://arxiv.org/ps/astro-ph/9904114v1>

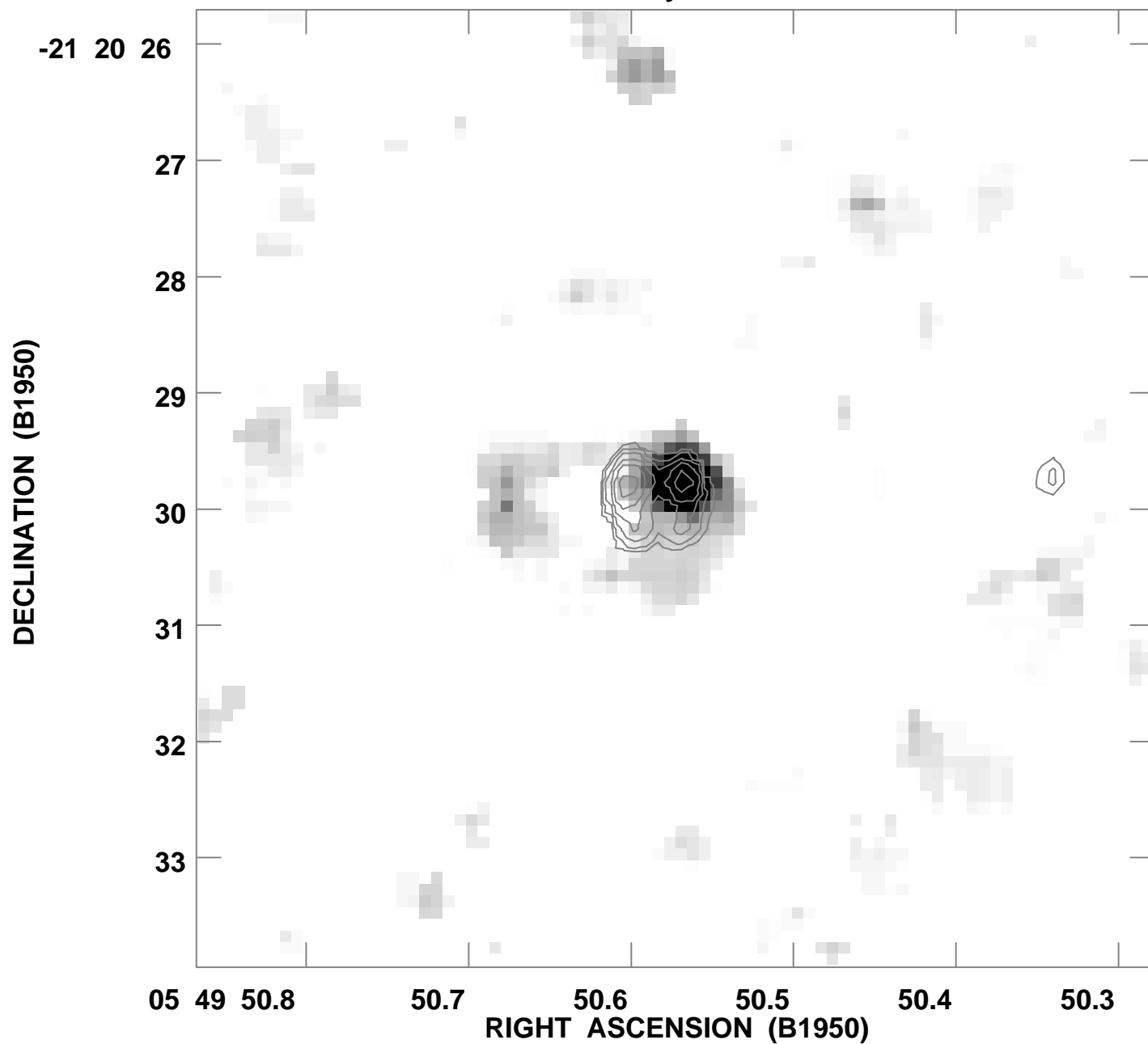
GREY: 0445+097 HST PC F555W
CONT: 0445+097 Radio 15 Ghz



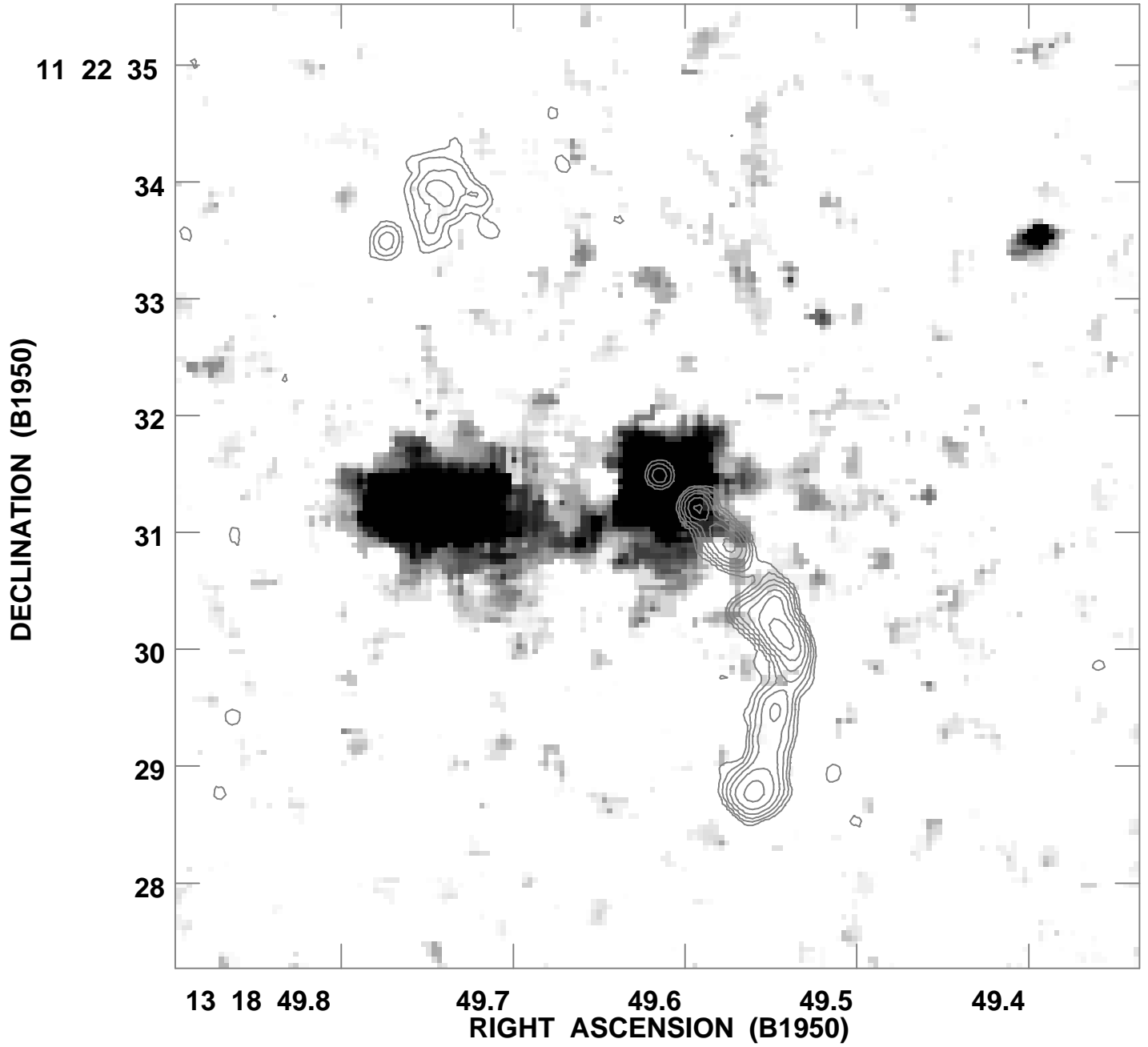
GREY: MRC0549-213 HST PC F555W
CONT: 0549-213 Radio 15 Ghz



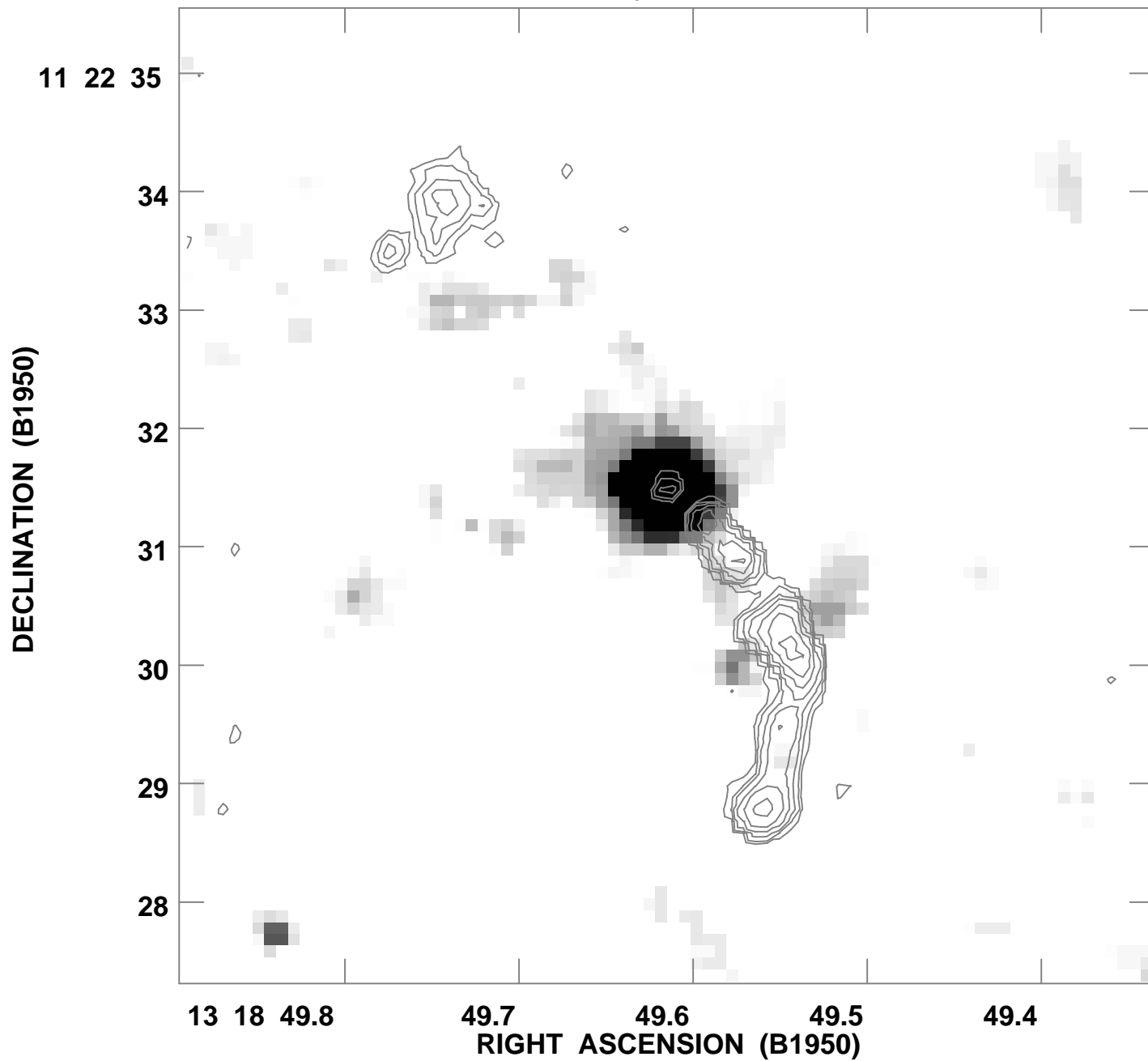
GREY: MRC0549-213 HST WFC Narrow-band
CONT: MRC0549-213 VLA A-array 15 Ghz



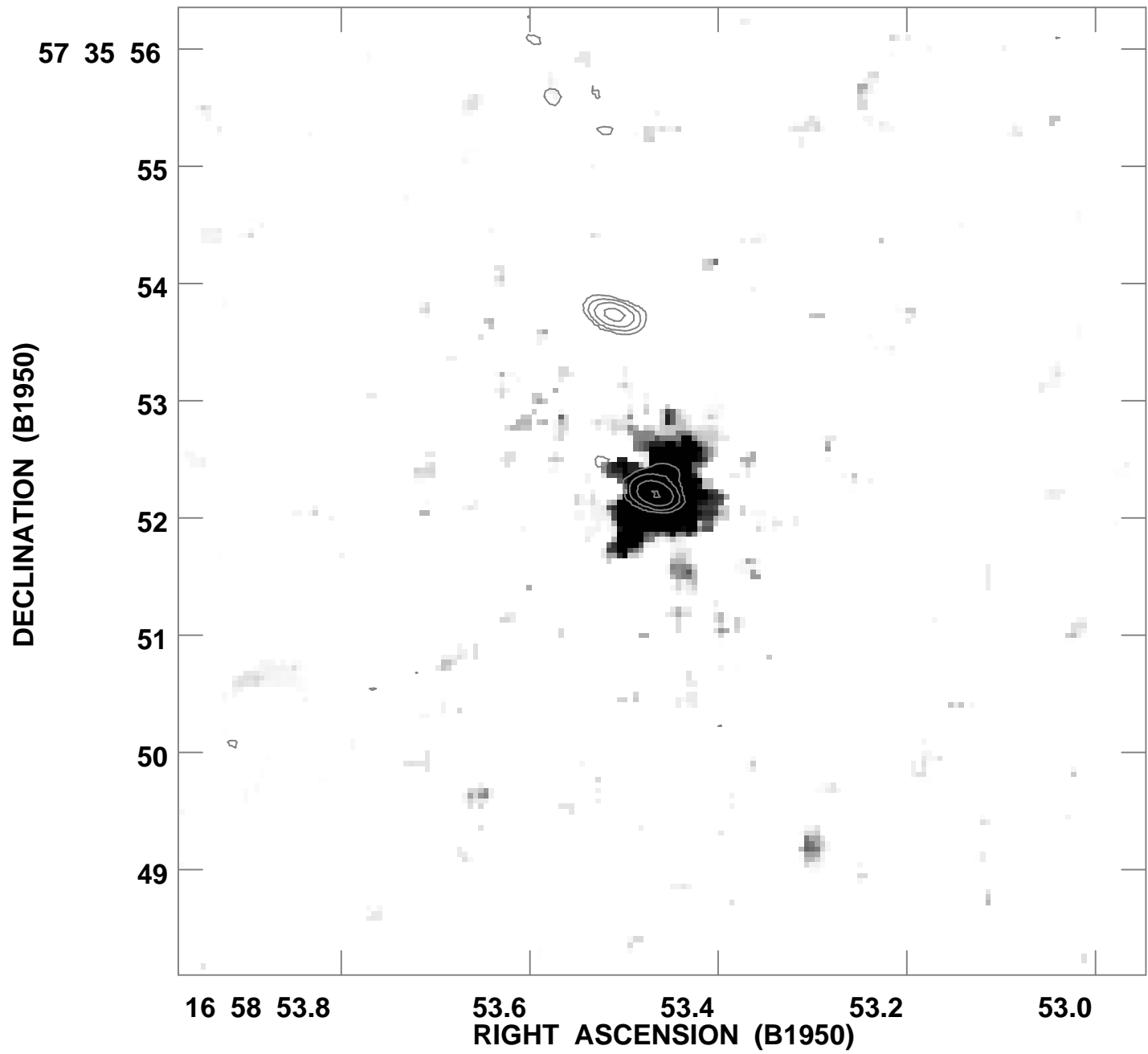
GREY: PKS1318+113 HST PC F555W
CONT: 1318+113 Radio 15 GhZ



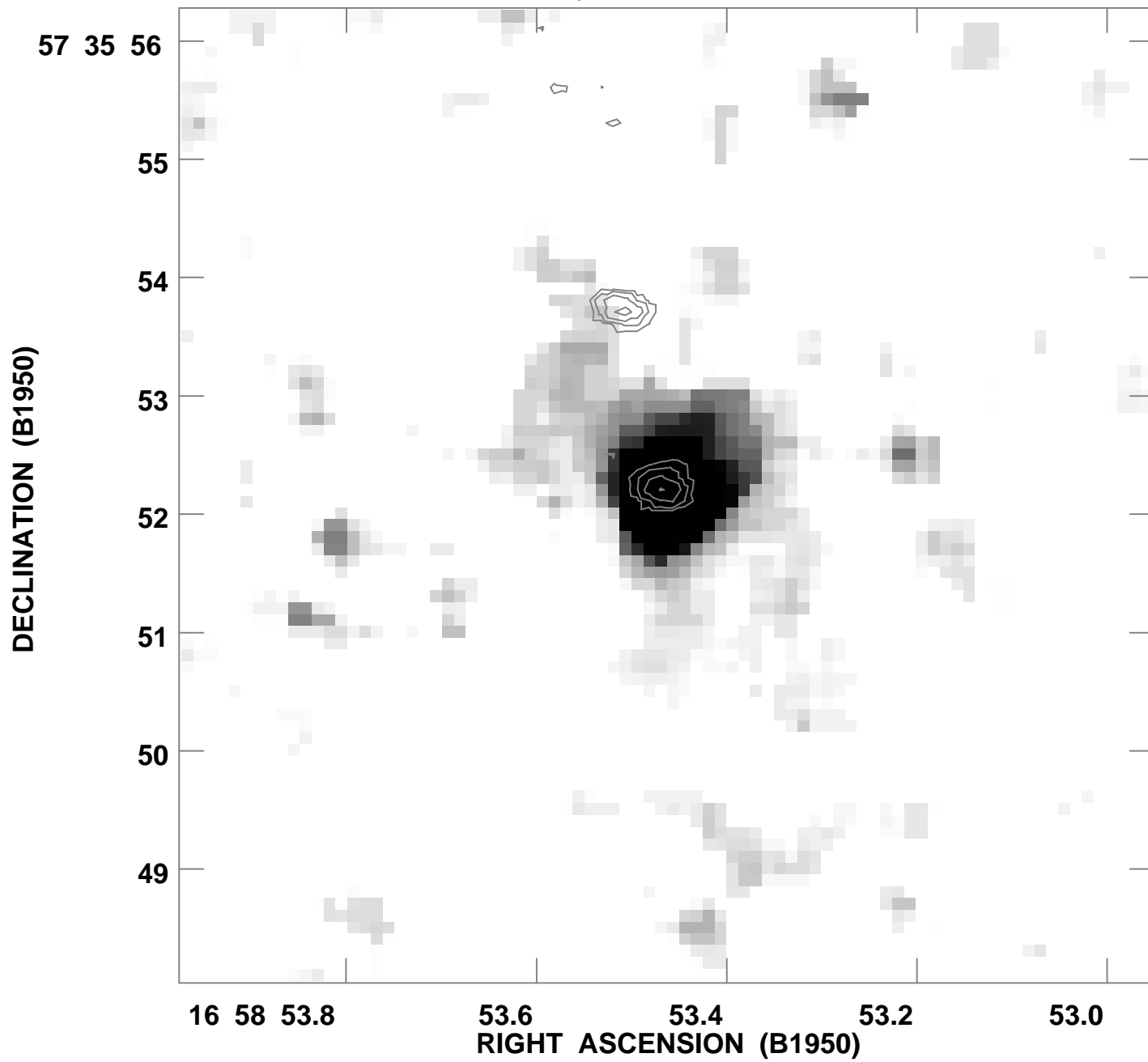
GREY: PKS1318+113 HST WFC Narrow-band
CONT: PKS1318+113 VLA A-array 15 Ghz



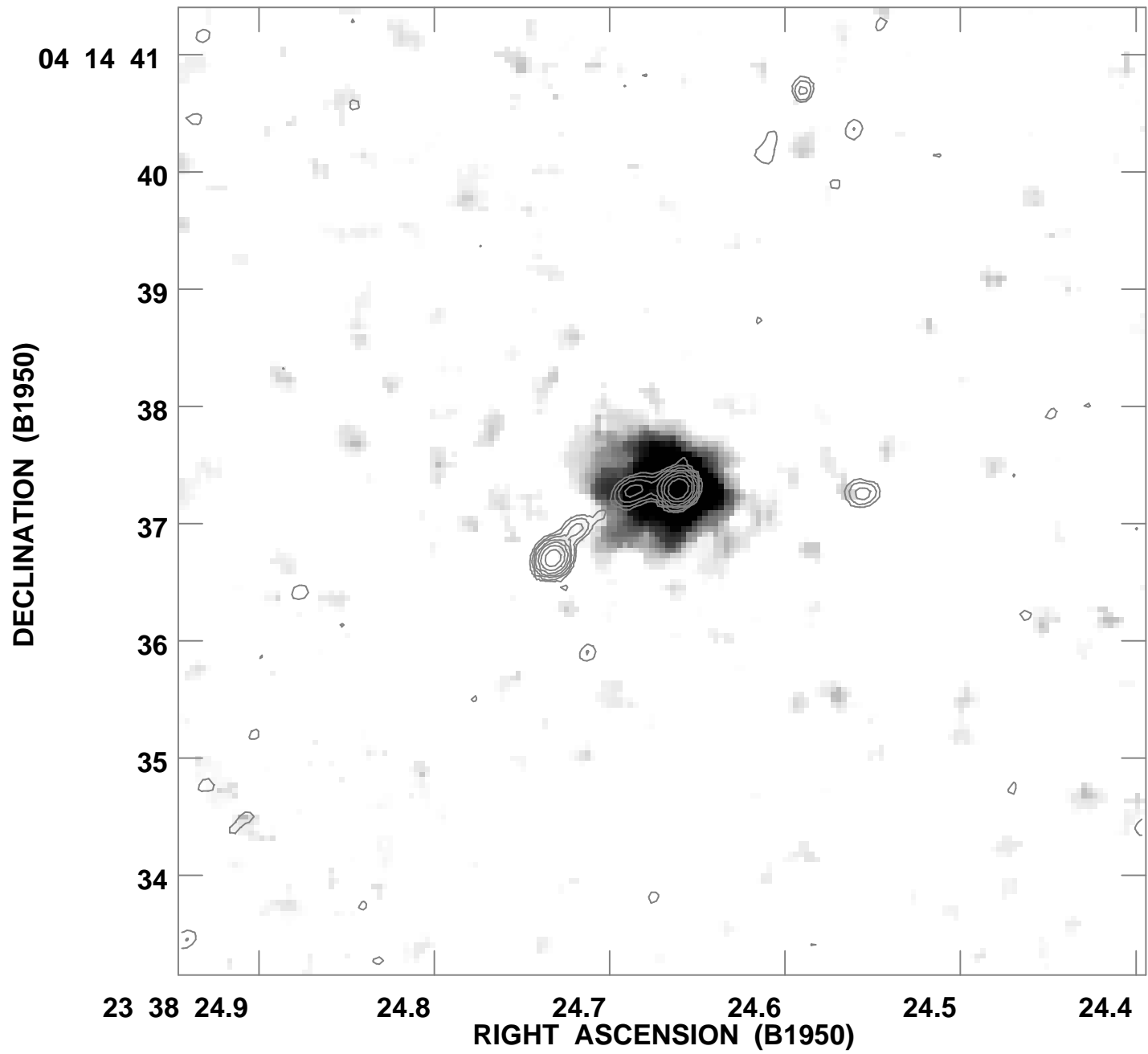
GREY: 4C 57.29 HST PC F555W
CONT: 4C 57.29 15 Ghz



GREY: 1658+575 HST WFC Narrow-band
CONT: 1658+575 VLA A-array 15 Ghz



GREY: PKS2338+042 HST PC F555W
CONT: PKS2338+042 VLA A-array 15 Ghz



GREY: PKS2338+042 HST PC Narrow-band
CONT: PKS2338+042 VLA A-array 15 Ghz

